Government of **Western Australia**
Department of **Mines and Petroleum**

RECORD 2012/2

GSWA 2012 EXTENDED ABSTRACTS
Promoting the prospectivity of Western Australia


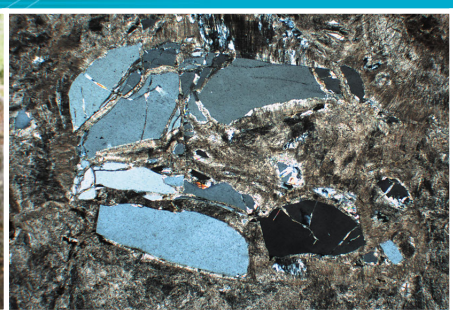


Geological Survey of Western Australia

Government of **Western Australia**
Department of **Mines and Petroleum**

Record 2012/2

GSWA 2012 EXTENDED ABSTRACTS

Promoting the prospectivity of Western Australia

February 2012

Perth 2012

Geological Survey of Western Australia

MINISTER FOR MINES AND PETROLEUM
Hon. Norman Moore MLC

DIRECTOR GENERAL, DEPARTMENT OF MINES AND PETROLEUM
Richard Sellers

EXECUTIVE DIRECTOR, GEOLOGICAL SURVEY OF WESTERN AUSTRALIA
Rick Rogerson

REFERENCE
The recommended reference for this publication is:

(a) For reference to an individual contribution:
Doublier, MP, Thébaud, N, Mole, D, Wingate, MTD, Kirkland, CL, Romano, SS and Wyche, S 2012 New data on the geological evolution and gold mineralization of the Southern Cross greenstone belt, in GSWA 2012 extended abstracts: promoting the prospectivity of Western Australia: Geological Survey of Western Australia, Record 2012/2, p. 1–2.

(b) For reference to the publication:
Geological Survey of Western Australia 2012, GSWA 2012 extended abstracts: promoting the prospectivity of Western Australia: Geological Survey of Western Australia, Record 2012/2, 36p.

National Library of Australia Card Number and ISBN PDF 978-1-74168-426-1; Print 978-1-74168-427-8

Published 2012 by Geological Survey of Western Australia
This Record is published in digital format (PDF) and is available online at <http://www.dmp.wa.gov.au/GSWApublications>.

Further details of geological products and maps produced by the Geological Survey of Western Australia are available from:
Information Centre
Department of Mines and Petroleum
100 Plain Street
EAST PERTH WESTERN AUSTRALIA 6004
Telephone: +61 8 9222 3459 Facsimile: +61 8 9222 3444
www.dmp.wa.gov.au/GSWApublications

Welcome to GSWA 2012

GSWA 2012, the Geological Survey of Western Australia's Open Day, aims to update geoscientists from the resources sector, researchers, and those involved in land-use planning on the latest GSWA activities and products.

The extensive poster displays and technical presentations are designed to highlight our ongoing programs. GSWA geoscientists will be available throughout the day to discuss the details of their project areas, the geology and mineralization of the State as a whole, and other aspects of the Survey's activities, products, and services.

We have again included poster displays from other geoscience agencies and research groups working in Western Australia, including CSIRO, Geoscience Australia, WA:ERA, MERIWA, the Centre for Exploration Targeting (CET), the John de Laeter Centre, and the Centre for 3D Mineral Mapping (C3DMM).

Programs being funded through the Western Australian State Government's Exploration Incentive Scheme (EIS) will feature prominently throughout the Open Day. 2011–12 marks the third full year of the EIS, which began in April 2009. Progress to date on EIS projects will be the subject of an Open Day presentation.

This year's Open Day program sees the introduction of two workshops, to be held during the lunch break. These workshops include a presentation of *GeoMap.WA* with the Explanatory Notes extension, and a sneak preview of the new web-based mapping tool, *GeoVIEW.WA*.

Your feedback on the Survey's work is welcome.

Rick Rogerson
Executive Director
February 2012

GSWA Seminar Program — February 2012, Fremantle

8.15 – 8.45	REGISTRATION	
8.45 – 9.00	Welcome and opening remarks	*Hon. Norman Moore MLC, Minister for Mines and Petroleum*
SESSION 1 Chair – Rick Rogerson		
9.00 – 9.15	Exploration Incentive Scheme (EIS) progress	*Rick Rogerson*
9.15 – 9.40	Structure, stratigraphy, magmatic evolution and timing of gold mineralization in the Southern Cross greenstone belt	*Michael Doublier*
Morning tea 9.40 – 10.50 in the display area		
SESSION 2 Chair – Don Flint		
10.50 – 11.15	2815–2800 Ma gabbros of the Murchison: A variety of mantle sources, magmatic processes and mineralization	*Tim Ivanic*
11.15 – 11.40	Metamorphic evolution of the west Yilgarn Craton	*Ben Goscombe (ITAR)*
11.40 – 12.05	Regional targeting criteria for gold in the Yilgarn Craton: which ones work and how well?	*Wally Witt (CET)*
Lunch 12.05 – 1.35		
Workshops in display area: 1.00 GeoMap.WA with Explanatory Notes extension		
1.15 GeoVIEW.WA		
SESSION 3 Chair – Stephen Bandy		
1.35 – 2.00	WA ASTER map	*Tom Cudahy (C3DMM)*
2.00 – 2.25	Structural development and mineralisation of the Edmund and Collier Basins, Capricorn Orogen	*Huntly Cutten*
2.25 – 2.50	What lies beneath – interpreting the Eucla Basement	*Catherine Spaggiari*
Afternoon tea 2.50 – 3.15 in the display area		
SESSION 4 Chair – Ian Tyler		
3.15 – 3.40	The west Musgrave Province mapping project – what's changed in seven years?	*Hugh Smithies*
3.40 – 4.05	Isotopic and geochemical data reveals both intracratonic and subduction-related phases in the early tectonic evolution of the Musgrave Province	*Chris Kirkland*
4.05 – 4.30	Multiscale dynamics of ore body formation	*Bruce Hobbs (CET)*
Sundowner 4.30 – 5.30		

Contents

New data on the geological evolution and gold mineralization of the Southern Cross greenstone belt

by

MP Doublier, N Thébaud[1], D Mole[1], MTD Wingate, CL Kirkland, SS Romano, S Wyche, and G Duclaux[2]

Introduction

Understanding the kinematic interaction between Archean greenstone belts and adjacent granites is crucial to constraining the formation and localization of major lode gold deposits. GSWA has performed detailed structural mapping in the central part of the Southern Cross Domain of the Youanmi Terrane, with a particular focus on the Southern Cross 1:100 000 map sheet. Southern Cross is a key area that contains well-preserved granite–gneiss domes separated by greenstone successions (Fig. 1), both of which have been affected by a complex geological history.

Stratigraphy

A detailed stratigraphy of the Southern Cross greenstone belt is difficult to establish due to its complex structure. However, the sequence broadly consists of a lower volcanic succession up to 5 km thick, overlain by a package of clastic sedimentary rocks at least 2 km thick. The lower part of the volcanic succession consists of tholeiitic and komatiitic basalt, whereas the upper part is dominated by komatiite. Several thin units of banded iron-formation are interbedded with the volcanic rocks, and minor amounts of gabbro have intruded this sequence. In the sedimentary package, the basal part is represented by black metamudstone ('black shale'), which is overlain by a mixed succession of psammitic and pelitic units, and minor quartzite and metaconglomerate.

Until recently, it was thought that the Southern Cross greenstones formed prior to 2.9 Ga, based on SHRIMP U–Pb ages of zircons from 'altered quartz porphyry sills' (Mueller and McNaughton, 2000) at the Southern Star (2934 ± 7 Ma; interpreted as a magmatic age) and Copperhead gold deposits (2912 ± 5 Ma; interpreted as a minimum age). However, a new SHRIMP U–Pb zircon age obtained from the lower part of the sedimentary succession, southeast of the Transvaal mine, indicates a maximum depositional age of 2702 ± 17 Ma for these rocks (Thébaud and Miller, 2009). This date suggests that at least the upper part of the stratigraphy is considerably younger than 2.9 Ga. Metasedimentary rocks from the Spotted Quoll mine in the Forrestania greenstone belt yield a maximum depositional age of 2832 ± 13 Ma, which again indicates sedimentary deposition younger than 2.9 Ga.

Structure and gold mineralization

The Southern Cross greenstone sequence is steeply dipping, and has been affected at various stages of the structural evolution by intense, commonly layer-parallel, shearing. This caused the formation of discrete shear zones traceable for tens of kilometres, and high-strain corridors up to several hundred metres wide. Furthermore, several generations of tight to isoclinal folds are developed in the area, some of which might represent sheath folds (Gee, 1995). These structures have complicated the internal structure of the Southern Cross greenstone belt. Although most gold deposits in the Southern Cross greenstone belt are located at contacts between different rock types, or between interflow and chemical sedimentary rocks, in proximity to the high magnesian and ultramafic part of the volcanic succession, gold mineralization is essentially controlled by shear zone networks (Gee, 1995).

Several studies have aimed to constrain the timing of gold mineralization in the Southern Cross greenstone belt. Figure 2 shows new data from Marvel Loch, which constrains the age of terminal shearing along the Marvel Loch shear zone, and therefore the gold mineralization, to between c. 2635 and 2630 Ma (GSWA 199043, Mueller et al., 2004). A younger date obtained from the Corinthia deposit possibly represents a minimum age for mineralization, or else indicates a separate, younger, mineralization event.

Magmatism

The Southern Cross area has a long-lasting history of felsic magmatism (Qiu et al., 1999). Our new geochronology data, together with previously published data, indicate a composite character for the Ghooli Dome, recording about 150 m.y. of granite magmatism between c. 2780 and 2630 Ma.

1 Centre for Exploration Targeting, The University of Western Australia, 35 Stirling Highway, M006, Crawley WA 6009

2 CSIRO Earth Science and Resource Engineering, Australian Resources Research Centre, 26 Dick Perry Avenue, Kensington WA 6151

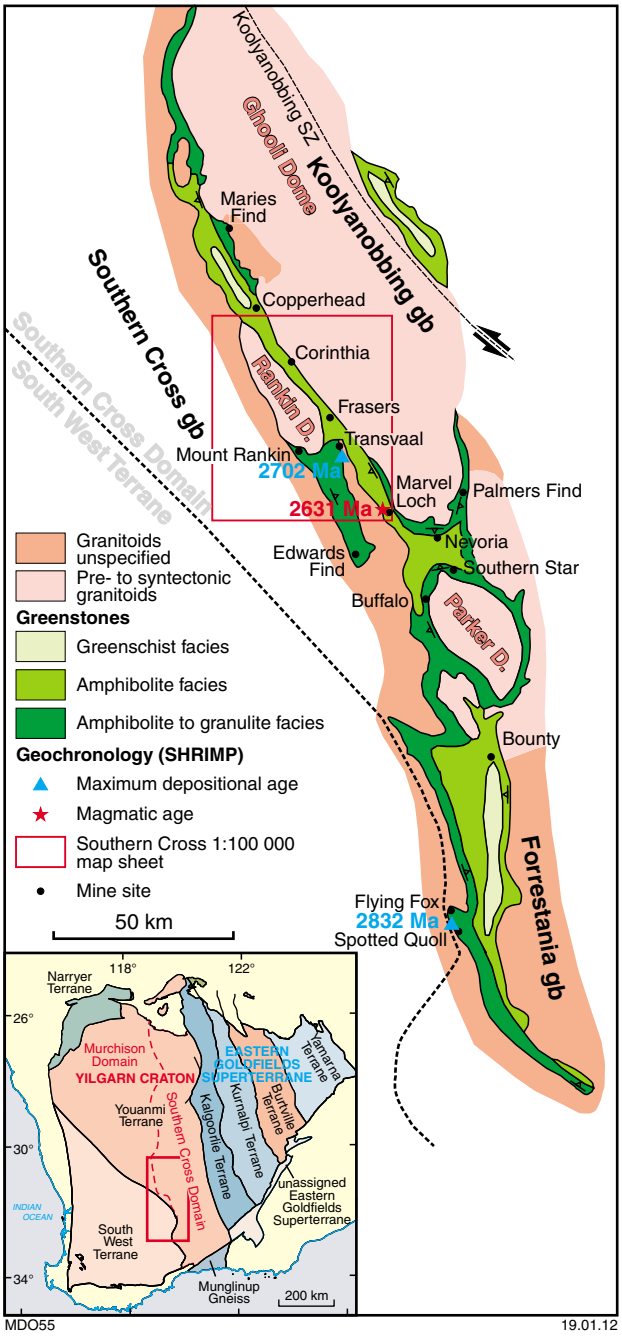

Figure 1. Geological overview of the Southern Cross region (after Ahmat, 1986; Mueller and McNaughton, 2000), showing important mines and selected geochronology sample sites. Abbreviations used in figure: SZ —shear zone; gb — greenstone belt; D. — dome.

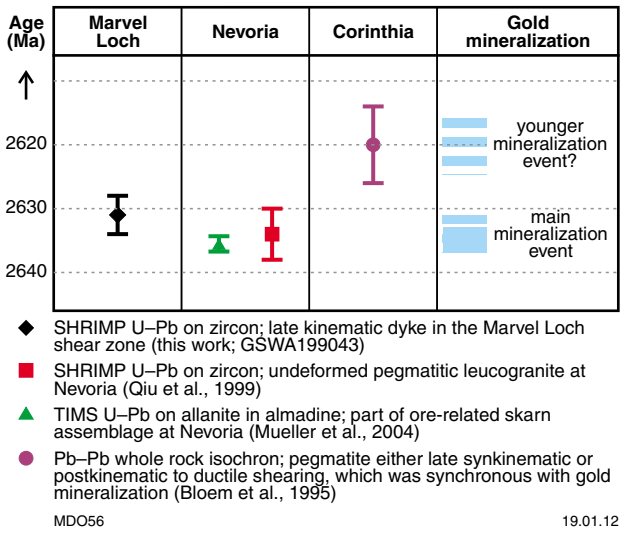

Figure 2. Timing constraints on gold mineralization

Future work

The structural framework, metamorphic history, and the relative timing of granite emplacement and mineralization relative to orogenic events, are critical parameters for distinguishing between different processes associated with the formation of granite–greenstones and mineralized gold systems. The results of this field-based study are now being inputed into a set of 3D thermal–mechanical numerical simulations as part of an ARC Linkage project. Results of this work are expected to be published in the near future.

References

Ahmat, AL 1986, Metamorphic patterns in the greenstone belts of the Southern Cross Province, Western Australia, *in* Professional papers for 1984: Geological Survey of Western Australia, Report 19, p. 1–21.

Bloem, EJM, McNaughton, NJ, Grove, DI and Ridley, JR 1995, An indirect lead isotope age determination of gold mineralization at the Corinthia mine, Yilgarn Block, Western Australia: Australian Journal of Earth Sciences, v. 42, p. 447–451.

Gee, RD 1995, Regional geology of the Southern Cross greenstone belt, *in* Southern Cross greenstone belt geology and gold mines: extended abstracts *edited by* PJ Schwebel: Geoconferences (WA) Inc., Southern Cross, Western Australia, March 1995, p. 11–16.

Mueller, AG and McNaughton, NJ 2000, U–Pb ages constraining batholith emplacement, contact metamorphism, and the formation of gold and W–Mo skarns in the Southern Cross area, Yilgarn Craton, Western Australia: Economic Geology, v. 95, p. 1231–1258.

Mueller, AG, Nemchin, AA and Frei, R 2004, The Nevoria gold skarn deposit, Southern Cross greenstone belt, Western Australia: II. Pressure–temperature–time path and relationship to postorogenic granites: Economic Geology, v. 99, p. 453–478.

Qiu, YM, McNaughton, NJ, Groves, DI and Dalstra, HJ 1999, Ages of internal granitoids in the Southern Cross region, Yilgarn Craton, Western Australia, and their crustal evolution and tectonic implications: Australian Journal of Earth Sciences, v. 46, no. 6, p. 971–981.

Thebaud, N and Miller, J 2009, U–Pb age constrain on the siliciclastic sediments from the upper supracrustal cover in the Southern Cross greenstone belt, Youanmi Terrane, Western Australia, *in* Smart science for exploration and mining *edited by* PJ Williams: Society for geology applied to mineral deposits; 10th Biennial SGA Meeting, Townsville, Queensland, 17 August 2009, p. 960–962.

2815–2800 Ma mafic intrusions of the Murchison: a variety of mantle sources, magmatic processes, and mineralization

by

TJ Ivanic

Voluminous mafic–ultramafic layered intrusions in the central Murchison Domain of the Yilgarn Craton document the presence of coexisting hydrous and anhydrous mantle domains tapped during the late Mesoarchean. New geochemical and age data from the Windimurra, Youanmi, and Narndee Igneous Complexes in Western Australia highlight the diverse mantle melts and respective sources emplaced within a period of only 5–10 m.y. The Windimurra Igneous Complex shows very little evidence for contamination of any kind, and appears to be depleted mantle -like. In contrast, the Narndee Igneous Complex shows evidence for derivation from LREE (light rare earth elements)-enriched hydrous mantle material, and also lacks evidence for significant crustal interaction. Hence, differing mantle domains are envisaged for these two magmas: an initial anhydrous domain tapped at c. 2810 Ma was responsible for the Windimurra Igneous Complex and other Meeline Suite igneous complexes (e.g. Youanmi, Atley, and Barrambi Igneous Complexes); and a LREE and H_2O-enriched metasomatized domain at c. 2800 Ma was the source for the Narndee Igneous Complex.

Geological Setting

The Windimurra and Narndee Igneous Complexes are two distinctive layered mafic–ultramafic intrusions in the Murchison Domain of the Yilgarn Craton. Owing to their relatively good preservation, these complexes offer a potential window into the mantle during the late Mesoarchean. The complexes belong to the Meeline and Boodanoo Suites (respectively) of the c. 2815 to c. 2735 Ma Annean Supersuite. Their age and stratigraphic relationships have been poorly understood previously, but recently acquired U–Pb age data (Ivanic et al., 2010) indicate a significant mafic–ultramafic event at c. 2800 Ma that was responsible for the emplacement of voluminous intrusive complexes during this chaotic and relatively short-lived event.

The complexes of the Meeline and Boodanoo Suites (Fig. 1) formed as concentrically layered, inwardly dipping intrusions, now modified by strike-slip shear zones and brittle faulting. Recent seismic data reveal a broad, upward facing, conical form for the Windimurra Igneous Complex (Jones et al., in press). Strong reflectors within the lower parts of the complex indicate a well-layered and thick ultramafic zone down to approximately 7 km depth.

Geochemistry and mineralization

Primitive mantle -like trace element signatures emerge from the array of mafic–ultramafic rocks analysed in the Windimurra Igneous Complex, with LREE being only slightly depleted (Fig. 2a). In contrast, the rocks of the Narndee Igneous Complex indicate consistent, negatively sloped and LREE-enriched profiles (Fig. 2b). No primary hydrous mineral has been identified for the Windimurra magma (following Ahmat, 1986), whereas hornblende is abundant in the Narndee Igneous Complex (minor phlogopite has also been documented). The origin of water in the Narndee magma is suspected to be derived from the primordial mantle, owing to a lack of evidence of crustal–oceanic contamination (cf. Scowen, 1991). In addition, the curvature of boninitic REE signatures are not matched by the Narndee data (Fig. 2b), despite the presence of hydrous minerals; hence, evidence in support of an arc-affinity is presently lacking.

Iron–vanadium concentrations are extremely enriched in the upper zone of the Windimurra Igneous Complex; in comparison, the geochemical fractionation trend lacks significant iron enrichment at Narndee. In terms of PGE (platinum group element) content, it would be expected that Narndee harbors significant platinum; however, the 'U'-shaped PGE concentration patterns indicate that this magma was fractionated at depth within its feeder system. Whole-rock PGE data from the Windimurra Igneous Complex indicates that the PGE content is low on average, but has the potential for reef-like concentrations adjacent to localized zones of cumulate sulfide crystals.

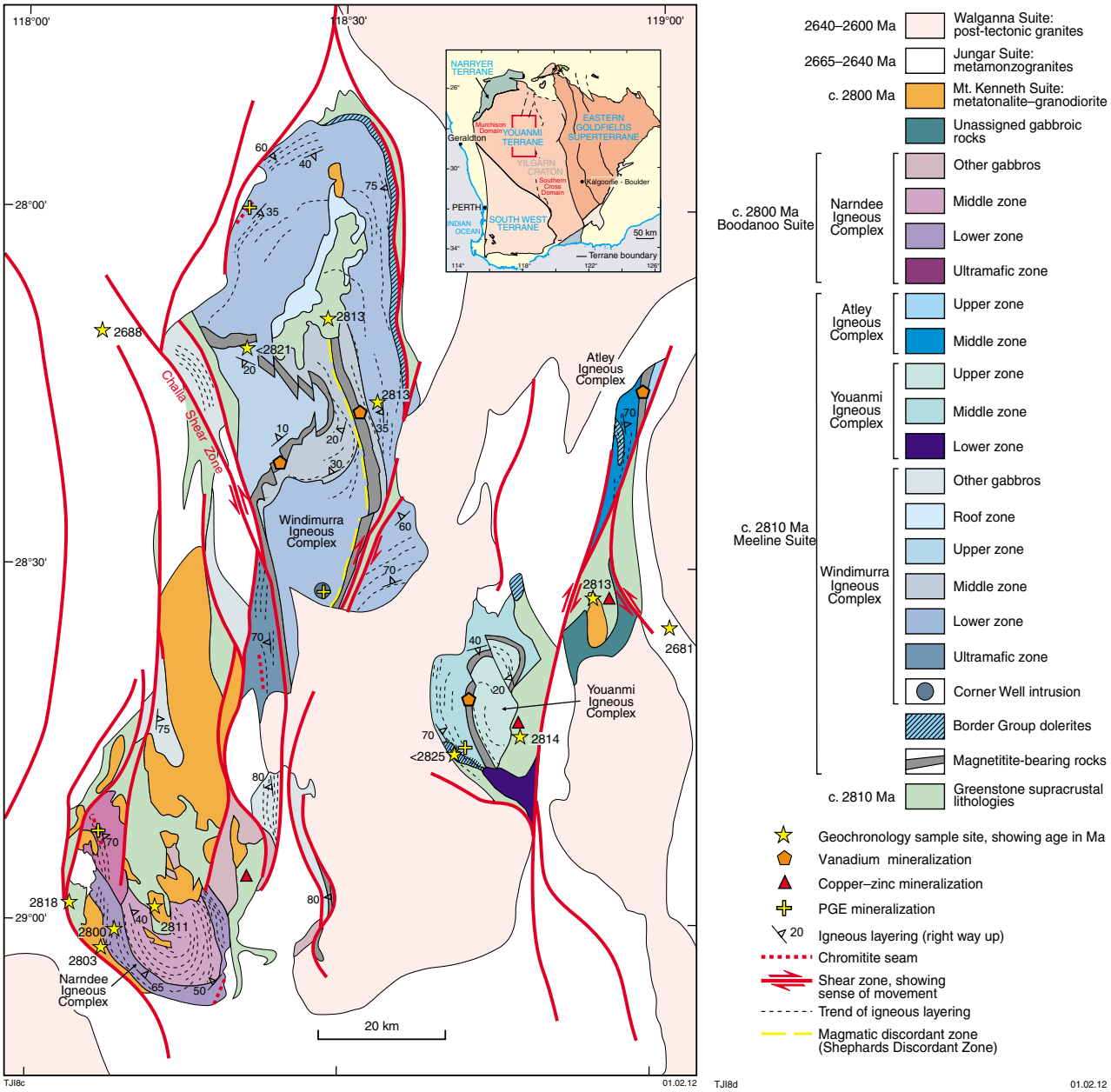

Figure 1. Interpreted geological bedrock sketch map of the eastern Murchison Domain, showing the Windimurra, Narndee, Youanmi, and Atley Igneous Complexes. Note the location of structures, and age and mineralization data. Zone nomenclature after Ivanic et al. (2010).

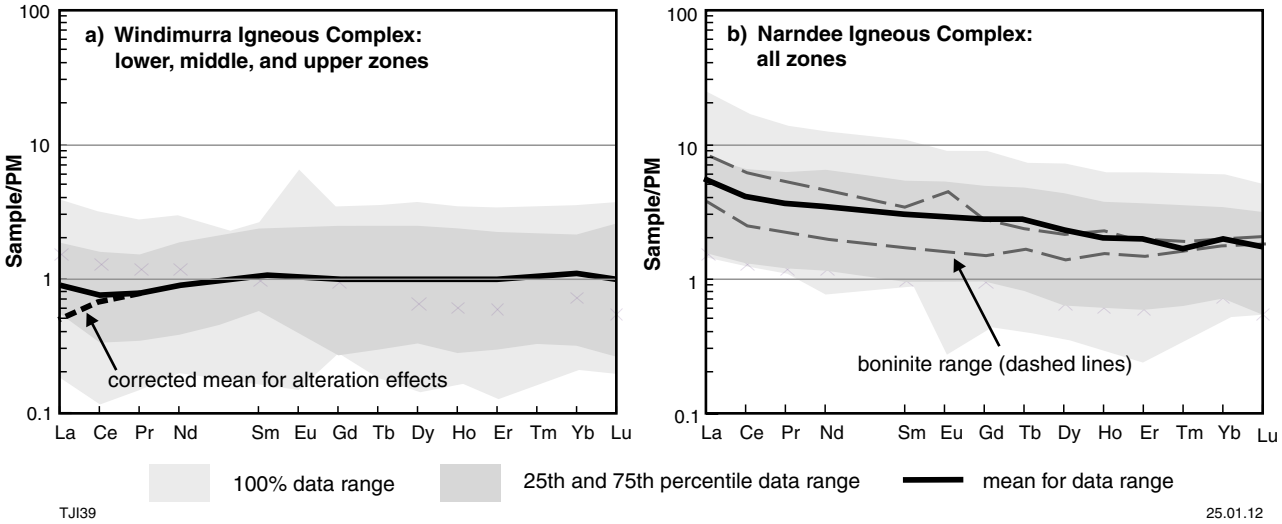

Figure 2. ***REE concentrations normalized to primitive mantle (PM) values (from Sun and McDonough, 1989) for the: (a) Windimurra Igneous Complex; (b) Narndee Igneous Complex.***

References

Ahmat, A 1986, Petrology, structure, regional geology and age of the gabbroic Windimurra complex, Western Australia: University of Western Australia, Perth, Western Australia, PhD thesis (unpublished), 279p.

Ivanic, TJ, Wingate, MTD, Kirkland, CL, Van Kranendonk, MJ and Wyche, S 2010, Age and significance of voluminous mafic–ultramafic magmatic events in the Murchison Domain, Yilgarn Craton: Australian Journal of Earth Sciences, v. 57, p. 597–614.

Jones, LEA, Ivanic, TJ and Costelloe, RD in press, Seismic reflection imaging of the mafic–ultramafic Windimurra Igneous Complex, Yilgarn Craton, Western Australia, *in* Unearthing new layers: Australian Society of Exploration Geophysicists; 22nd International Geophysical Conference and Exhibition, Brisbane, Queensland, 26–29 February 2012, Abstracts.

Scowen, PAH 1991, The geology and geochemistry of the Narndee intrusion: Australian National University, Canberra, Australian Capital Territory, PhD thesis (unpublished), 214p.

Sun, S-S and McDonough, WF 1989, Chemical and isotopic systematics of oceanic basalts: Implications for mantle composition and processes, *in* Magmatism in the ocean basins *edited by* AD Saunders, and MJ Norry: Geological Society of London, Special Publication 42, p. 313–345.

Thermobarometric evolution of subdomains within the western Yilgarn Craton

by

B Goscombe[1], R Blewett[2], D Foster[3], and B Wade[4]

Introduction

The western Yilgarn Craton (Fig. 1) preserves a long and complex metamorphic history, having >12 distinct periods of metamorphic paragenesis growth extending from the Paleoarchean to the Neoarchean. The dominant regional Neoarchean events are shared with the eastern Yilgarn Craton (Goscombe et al., 2007, 2009), although these events occurred in different tectonic settings and resulted in different metamorphic conditions. In addition, the northern, western, and southern margins of the craton have been variably reworked (regionally pervasive reworking) and reactivated (i.e. shear zones) as part of >10 distinct orogenic events from Paleoproterozoic to Cambrian in age, producing a wide range of metamorphic parageneses. The peak metamorphic conditions attained in key domains of the western Yilgarn Craton are summarized below. The peak conditions presented here are based on the pooling of pressure–temperature (P–T) calculations with self-similar results from small geographical subdomains. Pooled errors are ignored for clarity, but are typically ±10–30ºC and ±0.5 – 1.0 kb. The metamorphic constraints presented are preliminary and, at least at this stage in the research program, are not discussed within a chronologic, structural, and tectonic context.

Youanmi Terrane

Southern Cross Domain, north

The Edale Shear Zone, southeast of Sandstone in the north of the Southern Cross Domain of the Youanmi Terrane, experienced a wide range of low-pressure peak conditions — 524–607ºC, 2.2 – 4.5 kb, and temperature-over-depth ratios of 39–72ºC/km (n=14) — with clockwise P–T paths.

Along strike, the Illaara greenstone belt experienced peak conditions of 596ºC and 5.1 kb, with a temperature-over-depth ratio of 35ºC/km (n=2). Further along strike, the Ida greenstone belt experienced moderate-pressure peak conditions of 583–635ºC and 4.2 – 6.2 kb, temperature-over-depth ratios of 29–43ºC/km (n=3), and clockwise P–T paths.

The Marymia Inlier experienced low-pressure metamorphism in the east, and higher-pressure conditions in the west. Peak conditions in the east were approximately 561ºC and 3.0 kb, with a temperature-over-depth ratio of 53ºC/km (n=1); in the west, the conditions were 600ºC, 8.0 kb, and 21ºC/km (Gazley et al., 2011).

A single sample from the Atley greenstone belt experienced peak conditions of 450ºC and 4.2 kb, with a temperature-over-depth ratio of 31ºC/km. The Gum Creek greenstone belt experienced a moderate range of pressures: in lower-grade rocks, the peak conditions were 550ºC and 4.0 kb, with a temperature-over-depth ratio of 39ºC/km (n=1); higher-grade samples experienced higher-pressure peak conditions of 621ºC and 6.7 kb, with a temperature-over-depth ratio of 27ºC/km (n=2) and anticlockwise P–T paths. Granitoids in the Gum Creek area crystallized under very low pressures, at 1.2 kb. The Joyners Find, Red Handed Bore, Youanmi, and Poison Hills greenstone belts experienced similar peak conditions of 588–640ºC and 4.0 – 4.6 kb, with temperature-over-depth ratios of 38–44ºC/km (n=6); the Poison Hills greenstone belt has mineral parageneses indicating two metamorphic events. Lower-grade conditions in the Agnew–Wiluna greenstone belt were 517ºC, 3.8 kb, and 39ºC/km.

Southern Cross Domain, south

The Forrestania greenstone belt preserves evidence for events with a moderate range of pressures. Peak conditions in lower-pressure rocks were 503–661ºC and 2.8 – 5.2 kb, with temperature-over-depth ratios of 28–57ºC/km (n=18); however, a number of samples experienced higher-pressure peak conditions of 579–676ºC and 6.3 – 7.0 kb, with temperature-over-depth ratios of 24–31ºC/km (n=2), and clockwise and isothermal decompression P–T paths.

1 Integrated Terrane Analysis Research (ITAR), 18 Cambridge Rd, Aldgate SA 5154

2 Geoscience Australia, GPO Box 378, Canberra ACT 2601

3 Department of Geological Sciences, University of Florida, Gainesville Florida 32611, USA

4 Adelaide Microscopy, University of Adelaide, Adelaide SA 5005

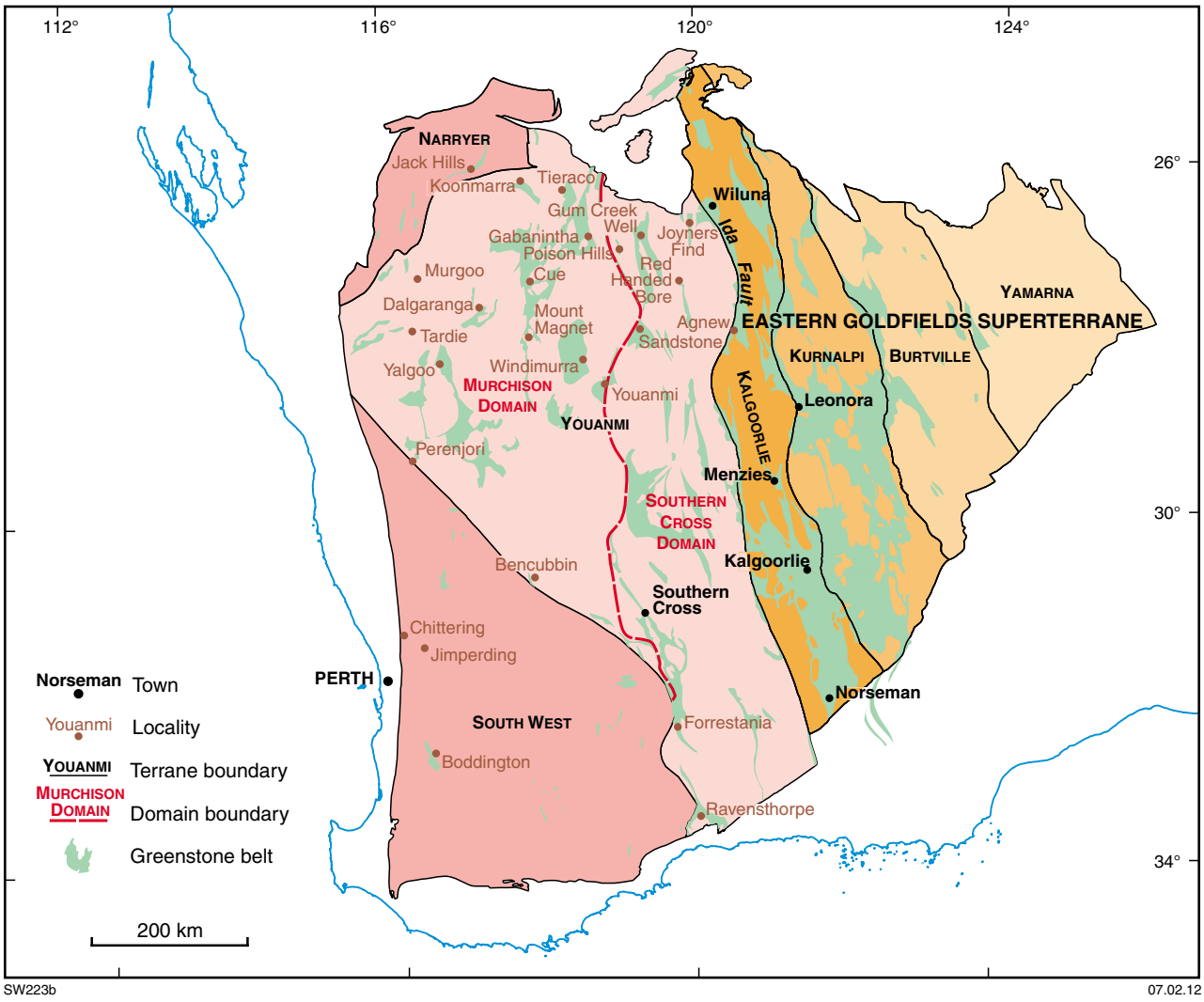

Figure 1. Terrane subdivision of the Yilgarn Craton, showing localities mentioned in the text

Ravensthorpe greenstone belt

The 'Carlingup Terrane' of Witt (1999), in the eastern part of the Ravensthorpe greenstone belt, experienced peak conditions of 566–580ºC and 4.5 – 5.0 kb, with temperature-over-depth ratios of 32–38ºC/km (n=10). Mineral parageneses indicate early anticlockwise P–T paths, followed by probable late clockwise P–T paths and secondary chloritoid growth, which may have been due to the loading of the Yilgarn margin during the Proterozoic Albany–Fraser events. A smaller number of samples experienced low-pressure peak conditions of 525–548ºC and 2.2 – 4.0 kb, with temperature-over-depth ratios of 38–71ºC/km (n=5), and clockwise P–T paths indicating isothermal decompression. The 'Cocanarup Terrane' of Witt (1999), on the western margin of the Ravensthorpe greenstone belt, experienced clockwise P–T paths with isothermal decompression, and peak conditions of 547–584ºC and 3.2 kb, with temperature-over-depth ratios of 49–52ºC/km (n=4). A few samples experienced higher-pressure peak conditions of 558–620ºC and 5.9 – 6.0 kb, with temperature-over-depth ratios of 27–30ºC km (n=2). The 'Ravensthorpe Terrane' of Witt (1999), in the central region of the greenstone belt, experienced peak conditions of 559–562ºC and 3.7 – 4.1 kb, with temperature-over-depth ratios of 39–43ºC/km (n=8). A few samples experienced higher-pressure peak conditions of 572–590ºC and 5.9 kb, with temperature-over-depth ratios of 28–29ºC/km (n=3). Both groupings experienced predominantly clockwise P–T paths with isothermal decompression, although a few samples have parageneses indicative of anticlockwise paths. The Manyutup Tonalite in the central 'Ravensthorpe Terrane' crystallized at low pressures — 3.0 – 5.1 kb (n=6) — and was subsequently buried and metamorphosed at 614–639ºC, 6.6 – 7.0 kb, and 26–27ºC/km (n=10).

Murchison Domain

Greenstones in the Murchison Domain of the Youanmi Terrane experienced a wide range of peak temperature conditions, all at low pressures. The lowest-grade conditions were 499ºC and 1.7 kb, with a temperature-over-depth ratio of 86ºC/km (n=4), and isothermal loading and anticlockwise P–T paths. Regional metamorphic peak conditions were 590–593ºC, 3.0 – 3.1 kb, and 55–56ºC km (n=3). The highest-grade peak conditions were 679ºC, 4.0 kb, and 51ºC/km (n=3).

The Koonmarra greenstone belt experienced peak conditions of 600ºC, 3.1 kb, and 55ºC/km (n=2), with decompressive cooling P–T paths. Greenstones around Murgoo, Tardie, and Tieraco had similar peak conditions, ranging 560–584ºC, 4.6 – 5.1 kb, and 33–35ºC/kb. Those around Perenjori and Bencubbin experienced higher grades but at similar pressures, with peak conditions of 631–632ºC, 4.1 – 4.7 kb, and 38–59ºC/kb.

The greenstones around Cue and Mount Magnet experienced at least two metamorphic events. Metamorphism associated with mineralization at Big Bell experienced a wide range in peak conditions — 543–648ºC and 4.6 – 4.9 kb, with temperature-over-depth ratios of 35–38ºC/km (n=9). Regional metamorphism elsewhere in the Cue region had typical peak conditions of 504–528ºC, 3.0 – 4.9 kb, and 30–45ºC/km (n=7), with isobaric cooling P–T paths, although a single sample has higher-pressure peak conditions of 575ºC, 6.4 kb, and 26ºC/km. Granitoids in this region crystallized under low-pressure conditions, at 1.9 kb (n=5).

The Dalgaranga greenstone belt experienced a wide range of peak temperature conditions, all at low pressures. The lowest-grade conditions detected were 494ºC and 2.0 kb, with a temperature-over-depth ratio of 76ºC/km (n=6), and ambiguous clockwise or anticlockwise P–T paths. Regional metamorphic peak conditions were 535–566ºC, 3.0 – 3.3 kb, and 51–53ºC/km (n=6), with clockwise and isothermal decompression P–T paths. Early gneissic metamorphism on the dome margins experienced peak conditions of 624ºC, 4.0 kb, and 45ºC/km (n=4).

The Yalgoo greenstone belt experienced a wide range in peak temperature conditions, all at low pressures. The lowest-grade conditions were 469ºC and 2.9 kb, with a temperature-over-depth ratio of 51ºC/km (n=4), and isobaric heating and isobaric cooling paths. Peak conditions were 552ºC, 3.3 kb, and 50ºC/km (n=4), with decompressive cooling P–T paths. Early gneissic metamorphism on the dome margins experienced peak conditions of 624ºC, 4.0 kb, and 45ºC/km (n=4).

Contact aureoles on the margins of mafic–ultramafic intrusive complexes, such as the Windimurra Igneous Complex, preserve the earliest and lowest-pressure metamorphic parageneses in the Youanmi Terrane. Windimurra contact aureoles preserve very low pressure conditions, ranging from 515ºC, 1.0 kb, and 147ºC/kb, to low-pressure granulites of 709ºC, 0.2 kb, and 844ºC km within a raft on the upper surface. The Gabanintha contact aureole, as elsewhere in the Murchison Domain, experienced peak temperatures, estimated in the literature, of 720–860ºC at unknown pressures (n=13).

Narryer Terrane

Narryer granulites preserve three distinct peak metamorphic conditions. Most P–T calculations for the subdomains have peak conditions in the range 665–681ºC and 4.1 – 4.5 kb, and temperature-over-depth ratios of 43–48ºC/km (n=10), with clockwise P–T paths. Higher-temperature peak conditions in some subdomains were 759–770ºC, 5.0 – 5.2 kb, and 42–43ºC/km (n=6), with clockwise P–T paths. An amphibolite-facies subdomain has peak conditions of 610ºC, 4.5 kb, and 39ºC/km (n=2), and a clockwise P–T path. Granitoids in the Narryer Terrane crystallized at pressures of 5.3 kb.

Retrograde shear zones are interpreted to have Proterozoic mineral parageneses. In the granulite terrane, these retrograde shear zones had metamorphic conditions ranging between 621ºC, 5.7 kb, and 31ºC/km (n=3), and 500ºC, 3.6 kb, and 40ºC/km (n=1). The Jack Hills greenstone belt is also interpreted to have Proterozoic mineral parageneses, with peak metamorphic conditions in different parts of the Jack Hills greenstone belt being 498–549ºC and 2.5 – 4.3 kb, with temperature-over-depth ratios of 36–61ºC/km (n=6), and clockwise P–T paths.

Transitional margins of the South West Terrane

Amphibolite-grade gneisses within the eastern transitional margin of the South West Terrane have peak conditions of 610–675ºC and 3.5 – 5.5 kb, with temperature-over-depth ratios of 34–50ºC/km (n=4). The northern transitional margin experienced both amphibolite- and granulite-facies metamorphism: granulite subdomains, including the Westonia greenstone belt, experienced peak conditions of 760–800ºC and 2.2 and 4.7 kb, with temperature-over-depth ratios of 103 and 46–49ºC/km (n=3). Amphibolite-grade gneisses also demonstrate a large range in pressures, with peak conditions of 536–615 and 630ºC, and 3.6 – 4.4 and 7.4 kb, with temperature-over-depth ratios of 34–43 and 24ºC/km (n=26).

South West Terrane

Granulite

Granulites in the eastern parts of the South West Terrane experienced peak conditions of 712–784ºC and 4.2 – 5.3 kb, with temperature-over-depth ratios of 44–52ºC/km (n=16), and isobaric cooling P–T paths. Granulites and granitoids in the western parts of the Southwest Terrane crystallized at 700–730ºC and 4.2 kb, with temperature-over-depth ratios of 48ºC/km (n=7). Mineral parageneses are ambiguous, but may indicate anticlockwise P–T paths. The Boddington greenstone belt experienced peak conditions of 500–600ºC, 2.0 –3.0 kb, and 57–71ºC/km (n=2).

Granulites from the ‘Lake Grace Terrane’ of Wilde (2001) preserve at least four distinct clusters of peak metamorphic conditions. The highest-pressure subdomain experienced peak conditions of 798ºC, 8.5 kb, and 27ºC/km (n=1),

with clockwise and isothermal decompression P–T paths. The highest-temperature subdomains experienced peak conditions of 754–852ºC, 5.4 – 6.9 kb, and 31–44ºC/km (n=8), with clockwise and isothermal decompression P–T paths. The lowest-pressure subdomains experienced peak conditions of 771–831ºC, 3.1 – 4.8 kb, and 50–71ºC/km (n=2), with ambiguous cooling paths. Finally, the lowest grade amphibolite-facies subdomains experienced peak conditions of 645–707ºC, 4.1 – 6.7 kb, and 28–49ºC/km (n=9), with isobaric cooling P–T path.

Granulites from the Jimperding greenstone belt also preserve at least four distinct clusters of peak metamorphic conditions. The highest-grade subdomains experienced peak conditions of 798–883ºC, 7.1 – 8.1 kb, and 30–35ºC/km (n=4), with clockwise P–T paths. Other subdomains with clockwise P–T paths experienced peak conditions of 810–826ºC, 5.8 kb, and 40–42ºC/km (n=6). The lowest-grade subdomains experienced peak conditions of 625–684ºC, 4.3–6.4 kb, and 31–42ºC/km (n=2), with isobaric cooling paths. Finally, subdomains with anticlockwise P–T paths experienced peak conditions of 713–807ºC, 3.6 – 5.0 kb, and 45–59ºC/km (n=8).

Chittering greenstone belt

Barrovian metapelite schists within the Chittering greenstone belt are interpreted to have Proterozoic or Cambrian metamorphic parageneses; there is currently no empirical evidence for earlier Archean parageneses or protoliths for these rocks. Nevertheless, the Barrovian-series main foliation envelops large, early garnet porphyroclasts, which are tentatively interpreted as relict Archean parageneses. Compositional isopleths from these garnet cores indicate low-pressure conditions of 549–560ºC, 4.8 – 4.9 kb, and 33ºC/km (n=7). Conversely, the main-foliation parageneses experienced high-pressure peak conditions of 565–572ºC, 8.0 – 10.6 kb, and 16–20ºC/km (n=9). P–T paths show isothermal loading, and very tight anticlockwise turn-around, followed by isothermal decompression.

‘Balingup Terrane’

Some rocks in the ‘Balingup Terrane’ of Wilde (2001) are strongly sheared and almost totally reworked to form Proterozoic metamorphic parageneses. Relict primary mineral grains within the mylonites and parageneses in the unsheared rocks are interpreted to be of Archean age. Archean assemblages preserve two peak metamorphic groupings: 1) conditions of 610–635ºC, 3.0 – 3.9 kb, and 45–60ºC/km (n=5), and 2) higher-pressure conditions of 592, 683, and 718ºC, 6.1 – 6.8 kb, and 28–31ºC/kb (n=8). Proterozoic mylonite assemblages in this terrane preserve peak metamorphic conditions of 597–670ºC, 5.7 – 6.9 kb, and 23–31ºC/km (n=38). Proterozoic P–T paths typically involved near-isothermal loading and a tight clockwise turn-around, followed by isothermal decompression.

Acknowledgements

The sponsors of the pmd*CRC Y4 project, the Geological Survey of Western Australia, Geoscience Australia, and Adelaide Microscopy are all gratefully acknowledged for their support and contributions. Steve Wyche is thanked for facilitating ongoing support of this long-term research program by the Geological Survey of Western Australia, and for providing samples contributed by Survey staff.

References

Goscombe, B, Blewett, RS, Czarnota, K, Maas, R and Groenewald, BA 2007, Broad thermobarometric evolution of the Eastern Goldfields Superterrane: *in* Proceedings of Geoconferences (WA) Inc. Kalgoorlie ’07 Conference: Geoscience Australia, Record 2007/14, p. 33–38.

Goscombe, BD, Blewett, RS, Czarnota, K, Groenewald, BA and Maas, R 2009, Metamorphic evolution and integrated terrane analysis of the Eastern Yilgarn Craton: rationale, methods, outcomes and interpretation: Geoscience Australia, Record 2009/23, 270p.

Gazley, MF, Vry, JK and Boorman, JC 2011, P–T evolution in greenstone-belt mafic amphibolites: an example from Plutonic gold mine, Marymia Inlier, Western Australia: Journal of Metamorphic Geology, v. 29, p. 685–697.

Wilde, SA 2001, Jimperding and Chittering metamorphic belts, southwestern Yilgarn Craton, Western Australia — a field guide: Geological Survey of Western Australia, Record 2001/12, 24p.

Witt, WK 1999, The Archaean Ravensthorpe Terrane, Western Australia: synvolcanic Cu–Au mineralization in a deformed island arc complex: Precambrian Research, v. 96, p. 143–181.

Regional targeting criteria for gold in the Yilgarn Craton: which ones work and how well?

by

WK Witt[1], A Ford[1], and W Hanrahan

Regional targeting criteria for gold in the Yilgarn Craton have been described and assessed using GIS spatial analysis, as part of the Yilgarn Gold Exploration Targeting Atlas, a collaborative project involving the Geological Survey of Western Australia (GSWA), the Centre for Exploration Targeting (CET), and several industry groups. These spatial analyses made use of GSWA's 1:500 000 interpreted bedrock geology shape files, legacy shape files inherited from the pmd*CRC, and Barrick Gold Corporation's gold deposit database. Twelve groups of containment analyses, and ten groups of proximity analyses, have been completed, and these form the basis of the results presented here. In proximity analyses, gold endowment (expressed in various forms) is plotted against buffer distance. Curves that peak in proximal buffers and decline with increasing buffer distance are interpreted to indicate a good relationship between gold abundance and the criterion under assessment. Erratic curves, and those in which gold endowment increases with increasing buffer distance, are regarded as poor targeting criteria for gold. The analyses have been variously carried out at the scale of the Yilgarn Craton, of individual provinces, or at the subprovince scale (superterrane, terrane, or domain), depending on the extent and reliability of the input data. Consistency of results between the eastern Yilgarn Craton, the central Yilgarn Craton, and the Murchison Domain in the northwestern Yilgarn Craton contributes to confidence in the results, especially where results are heavily influenced by a single deposit, such as the Golden Mile in the eastern Yilgarn Craton.

The most successful of the targeting criteria tested so far are: i) proximity to Mafic Group granitic intrusions; ii) proximity to regional faults and regional fault bends; and iii) regional fault density. Other useful criteria include: the presence of low-pressure, lower-greenschist M2 metamorphic domains; intermediate (3–5 km) greenstone thicknesses; vergence anomalies defined by regional faults; and late-stage basins. Other targeting criteria — including proximity to domes, regional strain partitioning, samarium–neodymium basement terranes, constriction zones, tomographic edges, and raw aeromagnetic and gravity worms — result in a greater chance of success than random exploration, but provide limited benefit to explorers compared to those previously listed criteria.

The targeting criterion producing the best results for gold exploration in the Yilgarn Craton is proximity to Mafic Group granitic rocks (Figs 1 and 2a). A 1 km buffer created around these intrusions captures 43.1% of the gold endowment (17.7% of deposits) in 0.85% of the area (a percentage endowment / percentage area (%endowment/%area) ratio of 50.4). Restricting the analysis to the Kalgoorlie and Kurnalpi Terranes of the eastern Yilgarn Craton results in a lower (but still very satisfactory) %endowment/%area ratio of 28.4. This result suggests a very strong relationship between gold and Mafic Group intrusions in the Murchison Domain (there are no Mafic Group granites documented in the central Yilgarn Craton, which is broadly equivalent to the Southern Cross Domain). Although lamprophyres are common in Archean gold deposits (Rock et al., 1989), by including lamprophyres with the Mafic Group granites in the Kalgoorlie plus Kurnalpi Terranes analysis, the %endowment/%area ratio is reduced to 11.3 (still a very good result). Note that the endowment versus buffer distance curves for Mafic Group granites (Fig. 2a) conform to that anticipated for a strong positive relationship between gold and proximity to Mafic Group granitic rocks, whereas the curves for High-Ca granitic rocks and Low-Ca granitic rocks do not.

Proximity analyses relating gold to regional faults produced the best results with a 1 – 1.5 km buffer. Results in terms of %endowment/%area are 5.90 (eastern Yilgarn Craton), 5.40 (central Yilgarn Craton), and 4.92 (Murchison Domain). Fault bends on the regional faults were generated digitally and these provided even better results, ranging from 49.0 for the central Yilgarn Craton, to 11.90 for the eastern Yilgarn Craton. Regional fault density was calculated, gridded, and contoured, resulting in seven to ten fault density bins. The resulting containment analyses relating gold to fault density produced a spectacular %endowment/%area ratio of 108.90 for the eastern Yilgarn Craton, but confidence in this result is tempered by the dominating effect of the Golden Mile. Results for the Murchison Domain (%endowment/%area ratio of 20.74) and central Yilgarn Craton (%endowment/%area ratio of 8.34) are considered more reliable.

1 Centre for Exploration Targeting, The University of Western Australia, Nedlands WA 6009

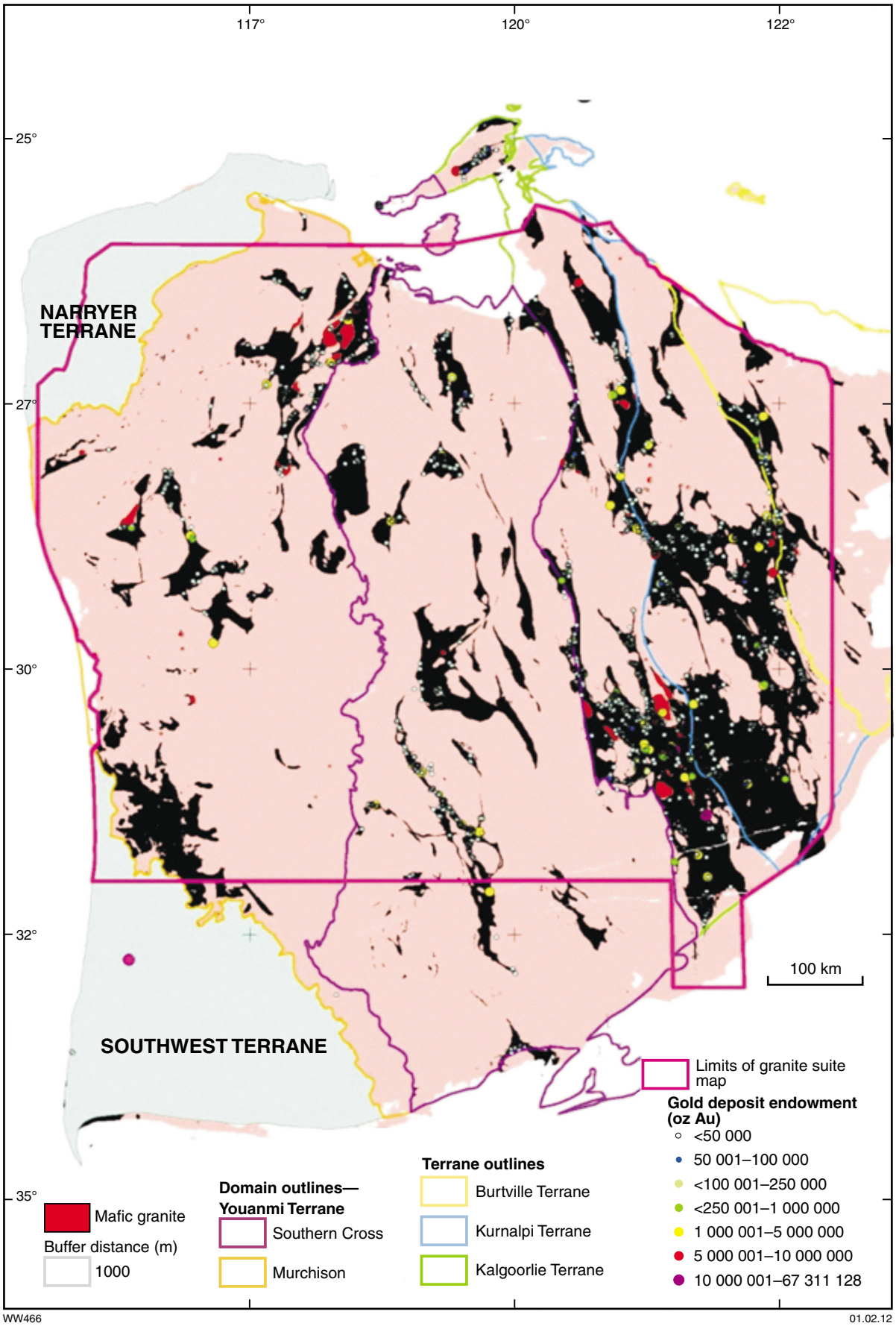

Figure 1. Map of the Yilgarn Craton, showing the distribution of gold deposits, and Mafic Group granites with 1000 m buffers

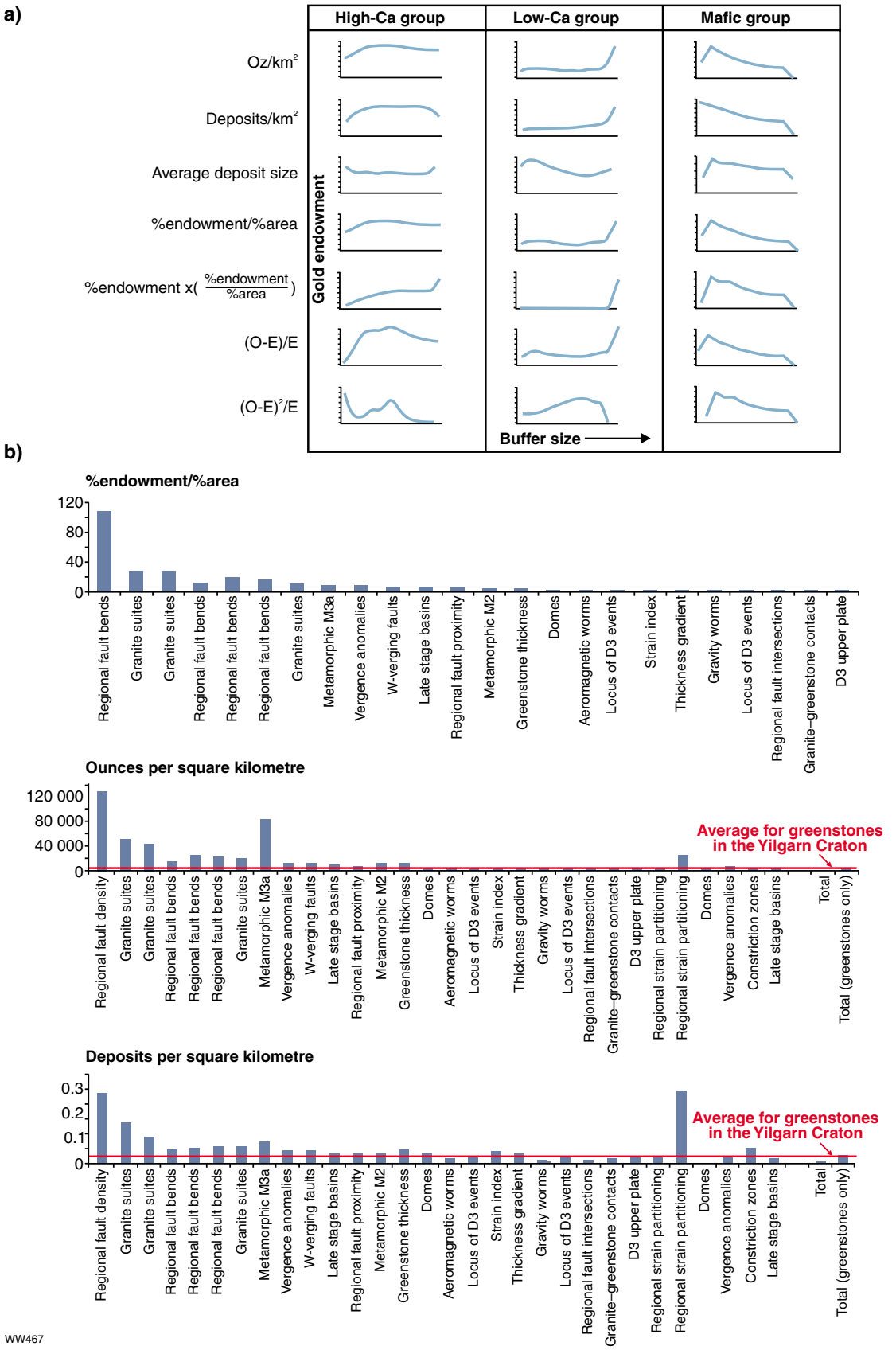

Figure 2. ***a) Tabulated results and curves relating gold endowment to buffers of various sizes, for High-Ca, Low-Ca, and Mafic Group granitoids, Yilgarn Craton. O represents the observed number of gold deposits or gold endowment (in ounces); E represents the expected number of gold deposits or gold endowment (in ounces); b) results of GIS spatial analyses, eastern Yilgarn Craton, ranked in terms of %endowment/%area for the most effective buffers***

Summary results of the GIS spatial analyses for the eastern Yilgarn Craton, the most data-rich area, are presented in Figure 2b, where the various targeting criteria are ranked in terms of %endowment/%area ratio, ounces of gold per square kilometre, and gold deposits per square kilometre. The analysis areas included both granites and greenstones in the eastern Yilgarn Craton. Those criteria that yielded less than the average ounces per square kilometre, or less than the average deposits per square kilometre for greenstones in the Eastern Yilgarn Craton (the red lines in Figure 2b), are considered to provide incremental benefit to explorers.

Ongoing work on the Yilgarn Gold Exploration Targeting Atlas covers exploration targeting and vectoring methods at both the district and deposit scales. At these larger scales, there is less of an emphasis on GIS spatial analysis, and a greater focus on case histories. This project is scheduled to be completed in May 2012, and the results will be freely available from the DMP website once GSWA publication processes have been completed.

References

Rock, NMS, Groves, DI, Perring, CS and Golding, SD 1989, Gold, lamprophyres and porphyries: what does their association mean?, *in* The Geology of Gold Deposits: the perspective in 1988 *edited by* RR Keayes, WRH Ramsay, and DI Groves: Economic Geology, Monograph 6, p. 609–625.

ROYALTIES FOR REGIONS
EXPLORATION INCENTIVE SCHEME

ASTER geoscience map of Western Australia

by

TJ Cudahy[1], M Caccetta[1], and S Collings[2]

Introduction

The public release of the ASTER geoscience maps of Western Australia, 2011 (14 in total, example shown in Fig. 1) represents an important benchmark. That is, it is the first and spatially largest public release of precompetitive geoscience information from the world's first and, to date, only operational, geoscience-tuned, global-mapping satellite system — the Japanese Advanced Spaceborne Thermal Emission and Reflection Radiometer (ASTER). The release of the Western Australian ASTER geoscience maps, chiefly mineralogy, represents 20 years of successful collaboration between many national and international organizations (see Acknowledgements).

This paper introduces the opportunities ASTER geoscience maps can provide for mineral exploration at the continental to prospect scales. It also provides background information on the ASTER system, in that it explains how and why the derived ASTER geoscience products were designed to capture accurate (for its resolution) mineral information. The key message is that the value of this new precompetitive geoscience information is dependent on the geological–mineralogical models developed and applied by users. It also underlines the fact that ASTER was designed to provide only broad mineral-group information, and not the content and physicochemistry of specific minerals, which would require a much higher spectral resolution.

Background

The Mineral Council of Australia (2006) recognized that Australia is an attractive place to explore, in part because of its growing national coverage of publicly available precompetitive geoscience data, such as airborne radiometric and magnetic data.

1 CSIRO Earth Science and Resource Engineering, Minerals Down Under Flagship, Western Australian Centre of Excellence for 3D Mineral Mapping, PO Box 1130, Bentley WA 6102.

2 CSIRO Mathematics, Informatics and Statistics, Leeuwin Centre, Private Bag No 5, Wembley WA 6913.

However, the Council also recognized that a new generation of geoscience data and knowledge is required to help reveal hidden prospectivity, and to reduce risk in 'frontier areas' across Australia. This was recently echoed in the findings of the 2010 Theo Murphy Think Tank, 'Searching the Deep Earth' (Australian Academy of Science, 2010), which specifically recognized the need to solve issues such as building a national map of the character of the cover, and developing tools to recognize the 'distal footprint' or far-field signatures of giant ore-systems. However, the exploration community has not previously had access to national precompetitive mineral information maps.

Over the last 10+ years, there have been developments in a new generation of geoscience-tuned spectral sensing systems, operating from drillcore, field, airborne, and space platforms, all of which can, in theory, be used to provide mineral information, even in three dimensions (<http://c3dmm.csiro.au>).

This emerging mineral-mapping technology measures natural electromagnetic radiation, in wavelengths extending from visible light (0.4–0.7 μm) through to thermal infrared (TIR; 7–12 μm), which is reflected or emitted from the top few microns of a material. Importantly, this wavelength range spans atmospheric windows that allow the measurement of diagnostic spectral features for minerals significant to the characterization of primary geology, metamorphism, metasomatic alteration, and weathering effects (<http://speclab.cr.usgs.gov/spectral-lib.html>).

However, these diagnostic mineral absorption features are often very narrow, such that hundreds of channels are theoretically required to measure the complete wealth of available mineral information, not only including the abundances of specific minerals, but also their chemical and structural variations. Such systems are often called 'hyperspectral', and include the Australian airborne HyMap system (<www.hyvista.com>), CSIRO's HyLogging suite (<http://www.csiro.au/Portals/Publications/Brochures--Fact-Sheets/hylogging.aspx>), and a number of hyperspectral satellites scheduled to be launched starting 2015 (<www.isiswg.org>).

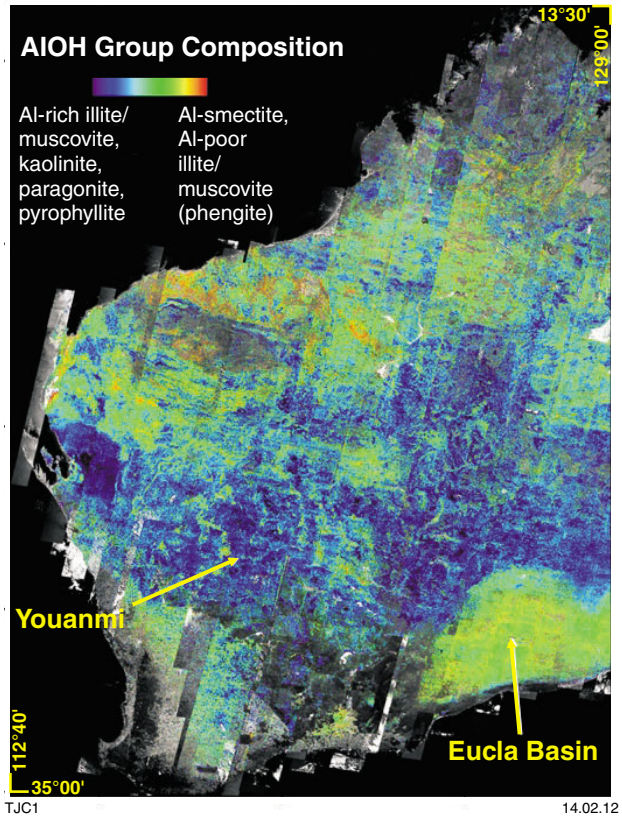

***Figure 1. Western Australian ASTER geoscience map of* AlOH Group Composition.**

ASTER

Japan's ASTER imaging system was launched onboard the USA's TERRA satellite platform in December 1999 (<www.ersdac.or.jp>; <http://asterweb.jpl.nasa.gov>). ASTER was included on this multisensor platform in large part because it provided a 'zoom' optical lens (15–90 m pixel resolution for 60 x 60 km wide scenes) for MODIS (Moderate Resolution Imaging Spectro-radiometer — 250–1000 m pixel resolution and a 2330 km wide swath). Both ASTER and MODIS are multispectral systems with 14 and 36 bands, respectively. MODIS was designed to measure parameters such as: concentration of atmospheric gases, like water vapour and ozone; chlorophyll absorption in photosynthesising biomass; and kinetic temperature. In contrast, ASTER was designed to map the Earth's land-surface composition (below 80° latitude), especially its mineral-group information, such as aluminium-clays, iron oxides, carbonates, and silica. That is, each ASTER band in the 1–12 µm region was positioned over a diagnostic spectral feature for a mineral group, such as ASTER Band 6, positioned at 2.2 µm to capture Al–OH bond vibration absorption in dioctahedral silicates like kaolinite, illite, and montmorillonite.

CSIRO's ASTER geoscience processing

In theory, only 15 independent parameters can be measured or mapped with ASTER's 14 available spectral bands though CSIRO's processing methods. These processing methods are based on developing multiple parameters and masks for each geoscience product, allowing additional geoscience products to be generated. Notes for the Version 1 ASTER geoscience products (Cudahy, 2011) show how each is generated, potential complications to their content, and examples of how they can be used geologically. The ASTER product notes also provide information about the qualitative and, in some cases, quantitative accuracy of each geoscience coverage. For example, in the absence of any vegetation, the RMSE (root mean square error) of iron oxide content is 11%, and that of aluminium-clay content is 5% (Haest et al., in press). Both green and dry vegetation complicate the accuracy of these interpretations, although future versions of the ASTER geoscience output are expected to reduce this error (Rodger and Cudahy, 2009).

Version 1 of the Western Australian ASTER geoscience maps only use ASTER's nine reflected bands (bands 1–9, spanning the 0.4 – 2.5 µm wavelength region) as suitable independent validation data were not available for the five TIR bands. To enable the validation of the shorter wavelength products, CSIRO used the national archive of the Hyperion satellite hyperspectral (covers the 0.4 – 2.5 µm wavelength region) imagery. In brief, the processing of the ASTER raw data (radiance-at-sensor) into geoscience coverages involved corrections and statistical cross-calibrations for instrument, solar irradiance, geometric, atmospheric, vegetation, and overlapping mineral absorption effects. The Western Australian ASTER mosaic used 1500 scenes, selected from CSIRO's archive of greater than 30 000 Australian scenes (sourced from Geoscience Australia, ERSDAC, NASA, and USGS). The final 14 digital Western Australian ASTER geoscience maps were then divided up into 1:1 000 000 scale map sheets (at ~100 Mb each map product) and converted to GIS-compatible formats (see below).

Version 1 of the ASTER geoscience map of Western Australia comprises three types of ASTER geoscience products, namely:

- Mineral group content, absorption depth relative to band/s outside of the absorption — ideally a continuum
- Mineral group composition, related to absorption geometry (wavelength)
- Mineral group index, which is sensitive to the material type, but not specifically its content or composition.

Figure 2 shows this distinction for the AlOH group, where content and compositional information plot along different trajectories for minerals either rich or poor in Al–OH vibrational bonds. Thus, an *AlOH Group Content* (ASTER bands: [5+7]/6) mask of more than two units is required

to more accurately map the composition of those pixels that contain AlOH minerals, such as kaolin, muscovite, and phengite. Without this mask to remove pixels with no apparent AlOH clay absorption, the resultant 'composition' image will show colour information for all pixels, but with much of this information incorrect. This explains why most ASTER mineral maps have many black (null data) pixels.

ASTER geoscience data access

The Western Australian ASTER geoscience maps are available to the public digitally, either as GIS-compatible images (e.g. in TIF and JPG format) or in image-processing software formats (e.g. BSQ with headers). The BSQ files are useful for those who want to set local colour stretches or apply filters to remove noise. The statewide ASTER mosaics were divided into 1:1 000 000 map sheets, with individual file sizes reduced to approximately 100 Mb each. The complete dataset, including the BSQ data (approximately 500 Gb), is available from the Department of Mines and Petroleum's Information Centre, as an external drive. The image (TIF and JPG format) data can be downloaded directly from CSIRO's website (<http://c3dmm.csiro.au>) and can be viewed on the Auscope Discovery Portal (<http://portal.auscope.org/portal/gmap.html>).

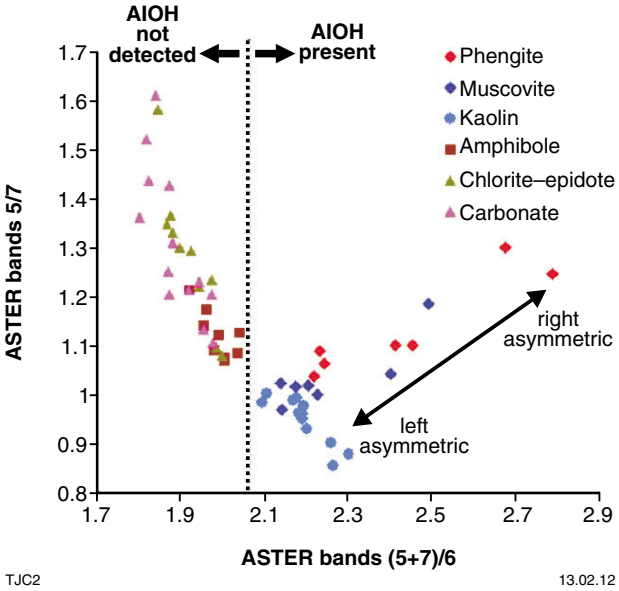

Figure 2. ***Scattergram of the ASTER-derived* AlOH Group Content *((B5+B7)/B6) versus the* AlOH Group Composition *(B5/B7) products, for a selection of pure minerals from the ENVI USGS mineral spectral library. From Cudahy et al. (2008).***

Geological demonstrations

The real value of these ASTER geoscience maps can be unlocked by applying geological models that accurately account for the mineralogical attributes of regolith cover, as well as the alteration footprints related to mineralized systems. That is, the maps are more than just colourful pictures for traditional photo-interpretation, although the *CSIRO Landsat TM Regolith Ratio* map was designed for this purpose. Instead, the ASTER mineral-group content, composition, and index products were specifically designed to capture both the potential of the ASTER spectral band configuration, and the quantitative information it can provide for mineral exploration purposes.

The ASTER geoscience product notes (Cudahy, 2011) provide more details on application, but as an example here, a useful exploration consideration could be mapping redox (reduced–oxidized) gradients (Neumayr et al., 2008), which can be gauged using the following ASTER coverages: (1) *Opaque Index*, which is sensitive to reduced rocks like graphitic shales, magnetite, and, if present at the surface, sulfides; (2) *Ferrous Iron Index*, which is sensitive to reduced iron (Fe^{2+}) bearing silicates (e.g. actinolite) and carbonates (e.g. ankerite, siderite); and (3) *Ferric Oxide Content*, which is sensitive to oxidized (Fe^{3+}) iron in the form of oxides (hematite and goethite) and sulfates (e.g. jarosite).

Figure 1 shows how the ASTER geoscience maps reveal mineralogical patterns at the continental scale. In this case, the ASTER *AlOH Group Composition* map shows patterns that reflect bedrock geology and/or climate. For example, the alkaline regolith conditions associated with the underlying carbonate rocks across the Eucla Basin have promoted the formation of soils rich in aluminium-smectite (warm colours in Fig. 1). In contrast, kaolin-rich soils are developed in a belt extending from 25–30°S latitude (cooler blue tones in Fig. 1), which straddles different bedrock types, including rocks of the Yilgarn Craton, Albany–Fraser Orogen, and the silica-rich sedimentary basins north of the Eucla Basin. These relatively silica-rich bedrock units are often associated with neutral to acid conditions, which promote kaolin (and hematite) development. However, the drier conditions of the 25–30°S latitude belt is likely more important as a controlling factor, as the same or similar bedrock found in latitudes less than 25°S and greater than 30°S preferentially develop illite–smectite (and goethite), presumably because the climate is wetter. Importantly, these ASTER mineralogy data are consistent with river sediment studies (Gingele and de Deckker, 2004), soil type studies (<http://www.asris.csiro.au>), and a recent Australian clay map modelled from a national soil spectral-data archive (Viscarra Rossel, 2011).

At the prospect-scale, and using the same basic mineralogical models, Figure 3 shows how the *Ferric Oxide Composition* map can be used to map transported versus in situ materials for an area near Youanmi, in the Murchison region. Based on a model where hematite, poorly ordered kaolin, and a lack of primary minerals are the mineralogical evidence for transported materials (Anand and Payne, 2002; Cudahy et al., 2005), the black vector outlining the hematite-rich (red) area in Figure 3b

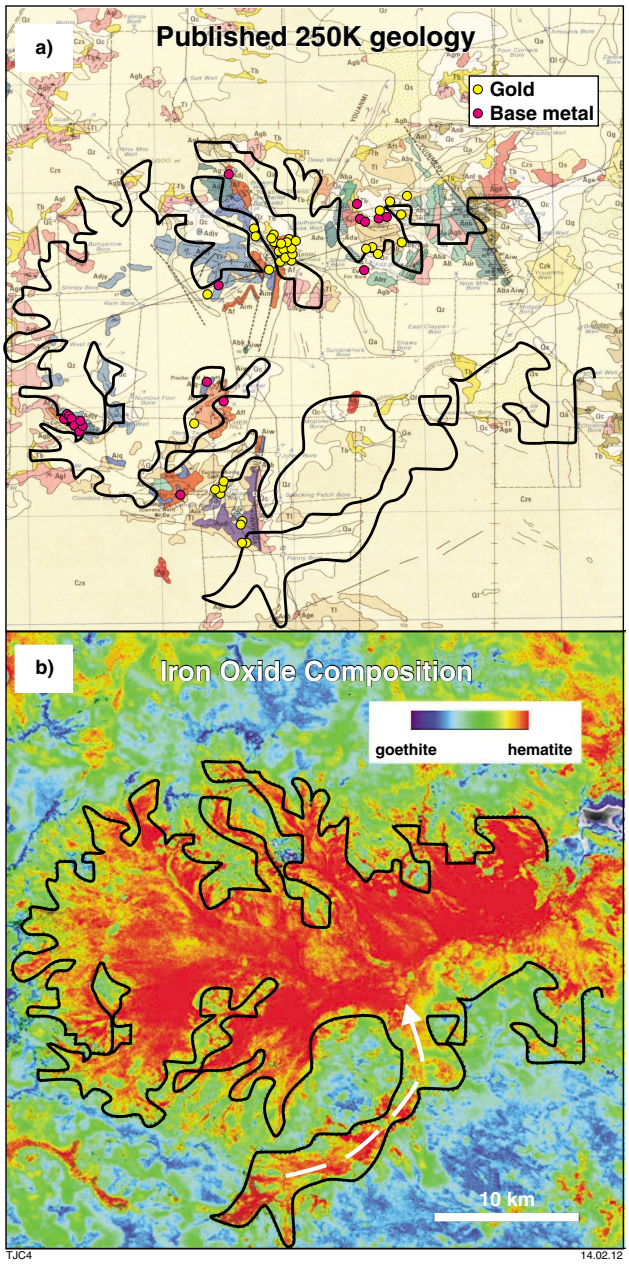

Figure 3. ***(a) Published 1:250 000 geology of the Youanmi area, with overlays of the gold and base metal occurrences, and a black vector marking the 'hematite-rich' areas shown in part b); (b) ASTER Iron Oxide Composition product, with hematite-rich in red and goethite-rich in blue. A 10 km scale bar is shown.***

represents transported material within a drainage basin. This vector has then been overlain on the published 1:250 000 geology in Figure 3a, showing the following points: (1) there is generally good correspondence between ASTER data and the alluvium/colluvium mapped for a drainage basin; (2) the published 1:250 000 geology appears to have missed a major drainage channel extending from the south (dashed curved white arrow; Fig. 3b); and (3), not unexpectedly, all the known mineral occurrences were found in areas of exposed bedrock geology.

This example shows that characterization of the regolith maps can be quickly compiled using this type of spatial mineral information, provided there is a suitable model of the regolith available. This enables the accurate digital mapping of transported 'cover' versus exposed (albeit variably weathered) bedrock, which will assist in devising more efficient sampling and drilling programs. It also highlights the possibility to reveal new exploration targets, such as uranium-calcrete or gold-placer paleochannels.

Figure 4 presents an example of how the ASTER mineral maps can be used to recognize 'metasomatic' alteration in naturally exposed greenstones. First, to set up the exploration model, a target host-rock for gold mineralization is selected to be a mafic rock, such as 'dolerite', which is consistent with the Golden Mile style of gold mineralization with superimposed potassium metasomatism and related iron-chlorite and 'sericite' development (Bateman and Hagemann, 2004). The known dolerites in the exploration area near Youanmi are highlighted by yellow vectors overlain on the 1:250 000 scale published geology (Fig. 4a). Figure 4b of the *Ferrous Iron in MgOH Group* map, shows that these mafic rocks comprise MgOH minerals (possibly including amphibole, chlorite, talc, serpentine, and/or carbonate), but that their ferrous iron contents vary from low (cool tones) to high (warm tones). This change in the Fe^{2+} content of the MgOH mineralogy can be a function of differentiation or layering within the mafic igneous rocks, or of cross-cutting hydrothermal alteration. The presence of Fe^{2+}-bearing chlorite could explain the pattern observed in the area highlighted by the white vector (Fig. 4b), making this area an exploration target as per the 'exploration model' being tested here. Note that the ASTER *FeOH Group Content* product should also be used to support this interpretation of chlorite.

Evidence for potassium metasomatism is offered by the *AlOH Group Composition* map (Fig. 4c), which has muscovite/phengite appearing as warmer tones. These tones appear over most of the highlighted dolerite units in the 1:250 000 scale published geology (Fig. 4a), and are also coincident with the area interpreted as chloritic (white vector; Fig. 4b). However, Cudahy (2011) notes that mixing with chlorite, carbonate, and dry vegetation can also influence the accuracy of the current *AlOH Group Composition* product, exaggerating warmer colours. Therefore, it is recommended that checks be made to help confirm the mineralogical interpretation, such as confirming (in this case) whether the 'muscovite/phengite' pixels also have high *AlOH Group Content*, low *FeOH Group Content*, and low *Green Vegetation Content*.

Figure 4b shows that this reduced 'fresh rock' signature extends >1 km to the southeast, over an area mapped as colluvium in the published 1:250 000 geology, and which is associated with copper mineralization. This provides an additional exploration target, as parts of this same area also contain muscovite–phengite (Fig. 4c).

This 'soft' geological modelling approach based on the ASTER mineral maps, can be transformed into 'hard' mathematical computer models reducing the need for visual, subjective interpretation, and capturing the intrinsic quantitative nature of these 'measured' data. This would

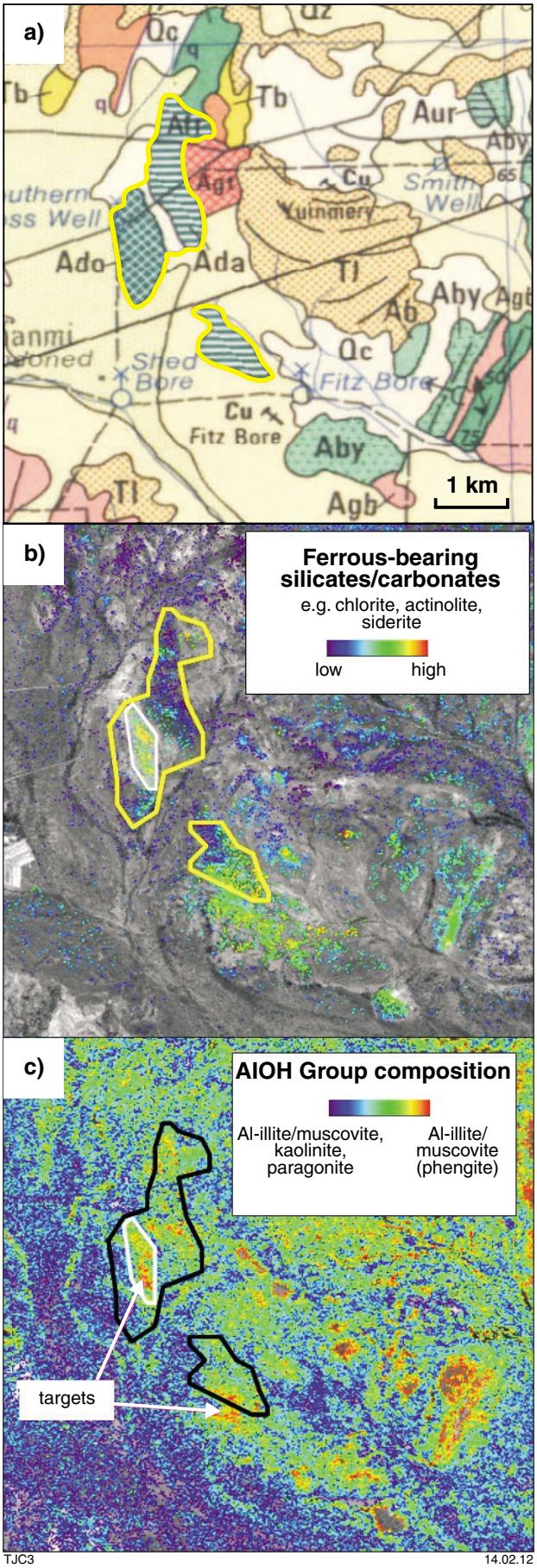

enable the rapid processing of large volumes of ASTER mineral maps, and other similar precompetitive digital spatial data, for regolith characterization and target generation in mineral exploration.

Closing points

This first public release of Australian ASTER geoscience products allows explorers in Western Australia to appreciate the geological value available from this new generation of 'geoscience-tuned' remote sensing data that can be applied from the continent to prospect scale. These data can be used for a wide range of mineral commodity styles, with their value essentially dependent on the geological models developed and tested by geoscientists. The National ASTER Geoscience map is scheduled for public release at the 34th International Geological Symposium, to be held in Brisbane, Queensland, in August 2012.

Acknowledgements

The development and delivery of the Western Australian ASTER geoscience maps has enjoyed the support of many organizations, including: CSIRO Earth Science and Resource Engineering; CSIRO Mathematics, Informatics and Statistics; CSIRO Minerals Down Under Flagship; Earth Remote Sensing and Data Applications Centre (Japan); NASA Jet Propulsion Laboratory (USA); United States Geological Survey; Western Australian Department of Mines and Petroleum, including the Geological Survey of Western Australia, and the Western Australian Government's Exploration Incentive Scheme; Western Australian Department of Commerce (through support of C3DMM); Geoscience Australia; Auscope; iVEC; and the Geological Surveys of Queensland and South Australia. To all of these organizations, we express our sincere thanks. Several people outside CSIRO have been critical in capturing the ASTER opportunity, namely Ian Tyler (GSWA), Mike Abrams (NASA), and Matilda Thomas (Geoscience Australia). Their efforts, as well as the significant contributions of many other individuals both inside and outside of CSIRO, have helped capture this important National (and global) geoscientific remote sensing opportunity.

Figure 4. ***(a) Published 1:250 000 geology of the Youanmi area, with yellow vector overlays showing the target host-rock, namely dolerite, used for a hypothetical exploration model; (b) ASTER product of* Ferrous Iron in MgOH Mineral Group*, which is used here to map distal alteration of Fe^{2+} chlorite and/or actinolite; (c) ASTER product of* AlOH Group Composition*, used to map areas of silicon-rich white mica (phengite), indicating proximal potassium-metasomatism.***

References

Anand, R and Paine, M 2002, Regolith geology of the Yilgarn Craton, Western Australia: implications for exploration: Australian Journal of Erath Sciences, v. 49, p. 3–162.

Australian Academy of Science 2010, Searching the deep Earth: the future of Australian resource discovery and utilisation: Theo Murphy High Flyers Think Tank 2010, Canberra, Australian Capital Territory, 19–20 August 2010, 56p.

Bateman, R and Hagemann, S 2004, Gold mineralisation throughout about 45 Ma of Archaean orogenisis: protracted flux of gold in the Golden Mike, Yilgarn Craton, Western Australia: Mineralium Desposita, v. 39, p. 536–559.

Cudahy, TJ, Caccetta, M, Cornelius, A, Hewson, RD, Wells, M, Skwarnecki, M, Halley, S, Hausknecht, P, Mason, P and Quigley, M 2005, Regolith geology and alteration mineral maps from new generation airborne and satellite remote sensing technologies; and Explanatory Notes for the Kalgoorlie–Kanowna 1:100,000 scale map sheet, remote sensing mineral maps: MERIWA, Report No. 252, 114p.

Cudahy, TJ, Jones, M, Thomas, M, Laukamp, C, Caccetta, M, Hewson, RD, Rodger, AD and Verrall, M 2008, Next generation mineral mapping: Queensland airborne HyMap and satellite ASTER surveys 2006–2008: CSIRO, Report P2007/364, 153p., <http://c3dmm.csiro.au/NGMM/index.html>.

Cudahy, TJ 2011, Satellite ASTER geoscience map of Western Australia: geoscience product notes, (Version 1) 15th November, 2011: CSIRO, viewed on 2 February 2012, <http://c3dmm.csiro.au/WA_ASTER/stage_1_geoscienceproductnotes.html>.

Gingele, FX and De Deckker, P 2004, Fingerprinting Australia's rivers with clay minerals and the application for the marine record of climate change: Australian Journal of Earth Sciences, v. 51, p. 339–348.

Haest, M, Cudahy, TJ, Laukamp, C and Gregory, S in press, Quantitative mineralogy from infrared spectroscopic data. 1. Validation of mineral abundance and composition scripts at the Rocklea iron deposit in Western Australia: Economic Geology, v. 107.

Minerals Council of Australia 2006, Geoscientific boost to minerals exploration: Media release, 14 August 2006: Minerals Council of Australia, viewed 2 February 2012, <http://www.minerals.org.au/__data/assets/pdf_file/0017/12266/mr006_25_energy.pdf>.

Neumayr, P, Walshe, J, Hagemann, S, Peterson, K, Roache, A, Frikken, P, Horn L and Halley, S 2008, Oxidized and reduced mineral assemblages in greenstone belt rocks of the St. Ives gold camp, Western Australia: vectors to high grade ore bodies in Archaean gold deposits?: Mineralium Deposita, v. 43, p. 363–371.

Rodger, A and Cudahy, T 2009, Vegetation corrected continuum depths at 2.20µm: an approach for hyperspectral sensors: Remote Sensing of Environment, v. 113, p. 2243–2257.

Viscarra Rossel, RA 2011, Fine-resolution multiscale mapping of clay minerals in Australian soils measured with near infrared spectra: Journal of Geophysical Research, v. 116, F04023, doi:10.1029/2011JF001977.

ROYALTIES FOR REGIONS
EXPLORATION INCENTIVE SCHEME

Structural development and mineralization of the western Edmund and Collier Basins

by

AM Thorne, SP Johnson, HN Cutten, and O Blay

Low-grade metasedimentary rocks of the Paleoproterozoic to Mesoproterozoic Edmund and Collier Basins form the youngest depositional elements within the Capricorn Orogen (Fig. 1). The succession comprises ~4 to 10 km of mainly fine-grained siliciclastic and carbonate sedimentary rocks that were deposited in a variety of shelf to basinal environments (Martin and Thorne, 2004). Sediments in the Edmund Basin were deposited unconformably on Paleoproterozoic basement rocks, including the Gascoyne Province, sometime between c. 1620 and c. 1465 Ma, based on the ages of the underlying Gascoyne Province and intrusive Narimbunna Dolerite. Sediments in the unconformably overlying Collier Basin were deposited across both the Paleoproterozoic basement and locally deformed sedimentary rocks of the Edmund Basin, after the Mutherbukin Tectonic Event at c. 1200 and before intrusion of the c. 1070 Ma Kulkatharra Dolerite.

Edmund Basin

The Edmund Basin corresponds to the present day outcrop of the Edmund Group. It contains four sedimentary packages whose depositional character was ultimately controlled by the primary orientation and repeated reactivation of major crustal structures in the Paleoproterozoic basement. These include the Talga, Godfrey, and Lyons River Faults in the west, and the Quartzite Well, Bujundunna, and Mount Vernon Faults in the east. Recently acquired deep seismic reflection data (Johnson et al., 2011a; Korsch et al., 2011) has highlighted the importance of the Talga, Godfrey, and Lyons River Faults, which are imaged as mantle-linked structures that dip steeply at the surface but become gently southward-dipping in mid- to lower-crustal levels. The Lyons River Fault has further significance in that it marks the early Paleoproterozoic crustal suture between the Glenburgh Terrane of the Gascoyne Province, and the Bandee Seismic Province of the Pilbara Craton.

Following the termination of the Mangaroon Orogeny at c. 1620 Ma, extensional reactivation took place on the Talga, Godfrey, Lyons River, Quartzite Well, Bunjindunna, and Mount Vernon Faults. Siliciclastic and carbonate sediments were deposited in the resulting half grabens, which show significant sediment thickness variations across the main structures. On the Pingandy Shelf to the north of the Talga Fault, the maximum thickness of Depostional Packages 1 and 2, in the lower part of the Edmund Group (Fig. 1), is ~1.5 km, whereas to the south they increase to ~3.75 km thick. Across the Godfrey Fault, Depositional Packages 1 and 2 increase in thickness from ~6 km to ~8.25 km. Depositional Packages 1 and 2 are also consistently thicker in the hangingwall of the basin-bounding extensional faults, suggesting that extensional downthrow on these major faults was toward the southwest. Depositional Package 2 is not present south of a line joining the Geegin Syncline with the Mount Vernon Fault, presumably having been incised and eroded away prior to the deposition of Depositional Package 3, which is up to 3 km thick in this area.

Collier Basin

Deposition in the Collier Basin (Depositional Packages 5 and 6 of the Collier Group) appears to have been less influenced by synsedimentary fault movements (Martin and Thorne, 2004), although the principal basin architecture parallels the main northwest–southeast to east–west structural trends seen within the underlying Edmund Basin and Gascoyne Province.

Mutherbukin Tectonic Event (1385–1200 Ma)

A major period of basin inversion took place during the 1385–1200 Ma Mutherbukin Tectonic Event (Johnson et al., 2011b), prior to deposition in the Collier Basin. In the underlying Gascoyne Province, this event was responsible for localized medium-grade metamorphism and deformation; however, evidence from the Edmund Basin has been more difficult to interpret, due to the very low grade nature of the metamorphism and difficulty in separating Mutherbukin-aged structures from similar, often coaxial, features formed during the later 1030–955 Ma Edmundian Orogeny.

Faults such as the Deverell Fault, in the eastern part of the Edmund Basin, have large, sinistral, strike-slip offsets, but show only small offsets in the overlying Collier Basin, suggesting pre-Edmundian Orogeny movements. These

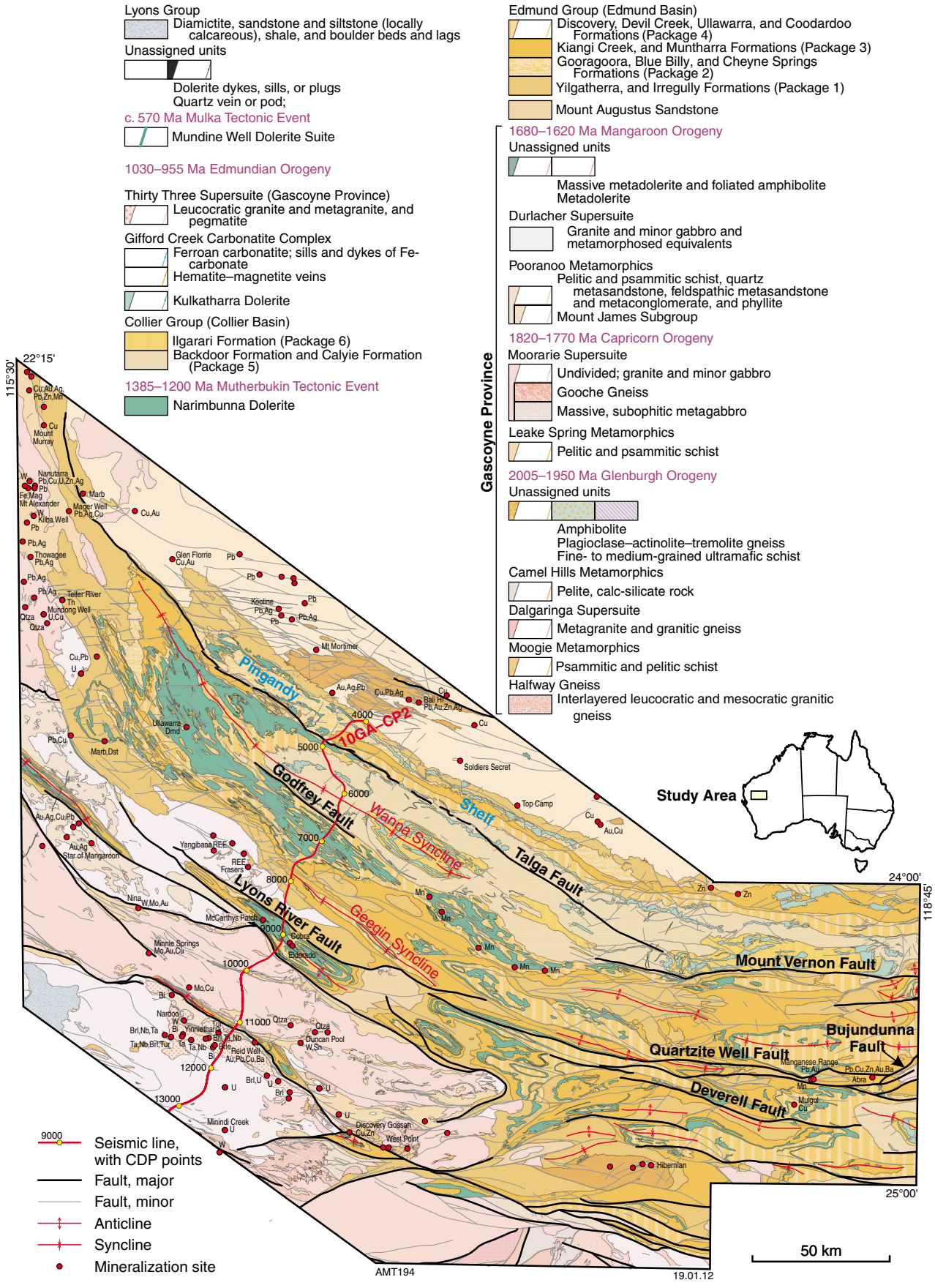

Figure 1. Geological map of the western Capricorn Orogen, showing the location of the principal structural elements within the Edmund and Collier Basins. The location of the deep seismic transect 10GA–CP2 is also shown.

features are replicated in the Wanna Syncline, where the intensity of faulting is significantly greater in the Edmund Basin than in the Collier Basin. Although Mutherbukin and Edmundian structures are generally coaxial, an exception occurs in the western Wanna Syncline, where rocks of the Edmund Group's Depositional Package 1 record localized, north-northwesterly vergent reverse faulting and associated folding of the Mutherbukin Tectonic Event, which has been refolded during later, northeasterly directed compression during the Edmundian Orogeny.

Due to the brittle nature of faulting in the Edmund Group, direct age constraints on fault movements are rare. However, authigenic illite from a fault gouge that displaces sandstone and siltstone beds of the Kiangi Creek Formation (Fig. 2) has been dated at 1171 ± 25 Ma using the $^{40}K/^{40}Ar$ method (GSWA, unpublished data), which is close to the younger age limit of the Mutherbukin Tectonic Event.

Edmundian Orogeny (1030–955 Ma)

The 1030–955 Ma Edmundian Orogeny was responsible for low to very low grade metamorphism and transpressional folding in the Edmund and Collier Basins. Martin et al. (2005) identified three distinct deformation events ($D1_{ed}$, $D2_{ed}$, and $D3_{ed}$), although $D3_{ed}$ is now considered to be related to the c. 570 Mulka Tectonic Event. The main $D1_{ed}$ event resulted from northeast–southwest transpression, whereas the later $D2_{ed}$ event was caused by weak east-southeast to west-northwest compression. It is currently unclear how the $D1_{ed}$ and $D2_{ed}$ folding and faulting events in the Edmund and Collier Basins relate to localized amphibolite-grade metamorphism, deformation, and granite intrusion in basement rocks of the Gascoyne Province (Sheppard et al., 2007).

In the western and central Edmund and Collier Basins, the fold and fault structures trend west–east to northwest–southeast, and are concordant with both the general basin architecture and the regional-scale structures in the underlying Gascoyne Province basement. Faults are steep, and often occur as zones of quartz veining or brecciated quartz in an ironstone matrix. Folds are generally upright and open, but are tightened adjacent to faults, and generally plunge gently to the northwest or southeast.

Figure 2. A small-scale reverse fault (~50 cm displacement) and associated folding in siltstone and thin-bedded sandstone of the Kiangi Creek Formation. $^{40}K/^{40}Ar$ geochronology on the fault gouge indicates that the structure formed during the latter stages of the Mutherbukin Tectonic Event.

Mulka Tectonic Event (c. 570 Ma)

The c. 570 Ma Mulka Tectonic Event is responsible for late-stage, dextral, brittle–ductile faults and shears, with associated quartz veins, in rocks of the Edmund and Collier Basins and Gascoyne Province. The faults also cut and offset dolerite dykes belonging to the c. 755 Ma Mundine Well Dolerite Suite (Sheppard et al., 2010).

Mineralization

The Edmund and Collier Basins have a history of minor gold, base metal, and phosphate production; however, a major orebody, the Abra polymetallic deposit, has also been discovered in these rocks. This deposit occurs in a fault-bounded structural corridor that links up with the mantle-tapping Lyons River Fault system, together with other prospective deposits, including vein-hosted gold mineralization at Cobra, and vein-hosted copper mineralization in Collier Group rocks at Ilgarari and Kumarina.

The formation of giant orebodies is often linked to the presence of crustal-scale plumbing systems that concentrate fluids, energy, and metals into specific sites in the crust. Many of these plumbing systems are intimately related to fossil subduction zones or old cratonic margins. The depositional and deformational history of the Edmund and Collier Basins was controlled by pre-existing crustal-scale structures in the underlying basement. These structures have also exercised a strong control on mineralization, with the multiply reactivated Paleoproterozoic fossil suture zone along the Lyons River Fault, in particular, appearing to have played a key role in orebody development (Tyler et al., 2011).

References

Johnson, SP, Cutten, HN, Tyler, IM, Korsch, RJ, Thorne, AM, Blay, O, Kennett, BLN, Blewett, RS, Joly, A, Dentith, MC, Aitken, ARA, Goodwin, J, Salmon, M, Reading, A, Boren, G, Ross, J, Costelloe, RD and Fomin, T 2011a, Preliminary interpretation of deep seismic reflection lines 10GA–CP2 and 10GA–CP3: crustal architecture of the Gascoyne Province, and Edmund and Collier Basins, *in* Capricorn Orogen seismic and magnetotelluric (MT) workshop 2011: extended abstracts (preliminary edition) *edited by* SP Johnson, AM Thorne, and IM Tyler: Geological Survey of Western Australia, Record 2011/25, p. 49–60.

Johnson, SP, Sheppard, S, Thorne, AM, Rasmussen, B, Fletcher, IR, Wingate, MTD and Cutten, HN 2011b, The role of the 1280–1250 Ma Mutherbukin Tectonic Event in shaping the crustal architecture and mineralization history of the Capricorn Orogen, *in* GSWA 2011 extended abstracts: promoting the prospectivity of Western Australia: Geological Survey of Western Australia, Record 2011/2, p. 1–3.

Korsch, RJ, Johnson, SP, Tyler, IM, Thorne, AM, Blewett, RS, Cutten, HN, Joly, A, Dentith, MC, Aitken, ARA, Goodwin, J and Kennett, BLN 2011, Geodynamic implications of the Capricorn deep seismic survey: from the Pilbara Craton to the Yilgarn Craton, *in* Capricorn Orogen seismic and magnetotelluric (MT) workshop 2011: extended abstracts (preliminary edition) *edited by* SP Johnson, AM Thorne, and IM Tyler: Geological Survey of Western Australia, Record 2011/25, p. 101–108.

Martin, DM and Thorne, AM 2004, Tectonic setting and basin evolution of the Bangemall Supergroup in the northwestern Capricorn Orogen: Precambrian Research, v. 128, p. 385–409.

Martin, DM, Sheppard, S and Thorne, AM 2005, Geology of the Maroonah, Ullawarra, Capricorn, Mangaroon, Edmund, and Elliott Creek 1:100 000 sheets: Geological Survey of Western Australia, 1:100 000 Geological Series Explanatory Notes, 65p.

Sheppard, S, Johnson, SP, Wingate, MTD, Kirkland, CL and Pirajno, F 2010, Explanatory Notes for the Gascoyne Province: Geological Survey of Western Australia, Perth, Western Australia, 336p.

Sheppard, S, Rasmussen, B, Muhling, JR, Farrell, TR and Fletcher, IR 2007, Grenvillian-aged orogenesis in the Palaeoproterozoic Gascoyne Complex, Western Australia: 1030–950 Ma reworking of the Proterozoic Capricorn Orogen: Journal of Metamorphic Geology, v. 25, p. 477–494.

Tyler, IM, Johnson, SP, Thorne, AM and Cutten, HN 2011, Implications of the Capricorn deep seismic survey for mineral systems, *in* Capricorn Orogen seismic and magnetotelluric (MT) workshop 2011: extended abstracts (preliminary edition) *edited by* SP Johnson, AM Thorne, and IM Tyler: Geological Survey of Western Australia, Record 2011/25, p. 109–114.

ROYALTIES FOR REGIONS
EXPLORATION INCENTIVE SCHEME

What lies beneath — interpreting the Eucla basement

by

CV Spaggiari, CL Kirkland, RH Smithies, and MTD Wingate

The Precambrian basement beneath the Eucla Basin represents one of Western Australia's most mysterious and darkest corners, which, until now, remained relatively unexplored due to a lack of knowledge and inherent high risk factors. New geophysical data and Exploration Incentive Scheme (EIS) co-funded drilling are helping to uncover the secrets of this basement, presenting new challenges to understanding the formation of southwestern Proterozoic Australia. The basement is covered by up to 500 m of sedimentary rocks belonging to the Cretaceous and Cenozoic Bight and Eucla Basins, and more deeply to the north by Neoproterozoic, Paleozoic, and Mesozoic sedimentary rocks.

Using geophysical data, the basement was previously divided from west to east into the Madura, Forrest, Waigen, and Coompana Provinces (Fig. 1; Shaw et al., 1996). The Waigen and Coompana Provinces lie predominantly within South Australia, adjacent to the Gawler Craton, and are completely under cover and poorly understood. Granitic gneiss from the Coompana Province (sampled from the Mallabie 1 drillhole in South Australia) has been dated at 1505 ± 7 Ma, interpreted as the igneous crystallization age of the granite protolith, which intruded into an unknown basement (Wade et al., 2007). The Madura Province lies adjacent to the Albany–Fraser Orogen, part of which also underlies the Eucla Basin (Fig. 1). In Western Australia, the division of the basement into separate provinces distinct from the Albany–Fraser Orogen will be tested through the interpretation of new aeromagnetic and gravity data, and by EIS co-funded exploration and stratigraphic drilling that will be sampled for geochronology and geochemistry.

Linking the Albany–Fraser Orogen to the Eucla basement

Current work on the Albany–Fraser Orogen has shown that it is dominated by Paleoproterozoic and Mesoproterozoic rocks that formed along, or close to, the margin of the Yilgarn Craton, resulting in successive episodes of reworking of that margin. Fragments of Archean crust, ranging from the kilometre-scale through to grain-sized (i.e. the isotopic record preserved in zircon) are interpreted as the rifted remnants of the Yilgarn Craton preserved within c. 1800 to 1650 Ma crust of the Biranup Zone. These fragments may have contained sources of economic minerals or elements, such as gold. Paleoproterozoic magmatic rocks of the Biranup Zone are interpreted to have intruded into the southern Yilgarn Craton during margin extension and rifting, possibly in a backarc setting, producing a series of linked basins across the Northern Foreland and Biranup Zone (i.e. the Barren Basin; Spaggiari et al., 2011). At least one tectonothermal event has been recognized during this period — the c. 1680 Ma Zanthus Event, which took place during the c. 1710 to 1650 Ma Biranup Orogeny (Kirkland et al., 2011; Spaggiari et al., 2011).

Previous interpretations of the Albany–Fraser Orogen have suggested the collision or accretion of exotic terranes, such as the Mawson Craton, and the formation of a magmatic arc in the Fraser Zone during the Mesoproterozoic Albany–Fraser Orogeny. Current U–Pb geochronology, whole-rock geochemistry, and Lu–Hf and Sm–Nd isotopic data do not support these interpretations — no exotic components, nor Mesoproterozoic magmatic arcs, have been recognized within the orogen. In addition, recently dated Paleoproterozoic metagranitic rocks within the eastern Nornalup Zone indicate continuation of that substrate eastwards from the Biranup Zone. The Mesoproterozoic Albany–Fraser Orogeny is divided into two stages: the first was a long-lived, widespread, coeval felsic and mafic magmatic event accompanied by deformation, and high-temperature and moderate- to high-pressure metamorphism (Stage I; c. 1345 to 1260 Ma); whereas the second stage was dominated by intense deformation, high-temperature and moderate-pressure metamorphism, and mostly felsic magmatism after c. 1200 Ma (Stage II; c. 1215 to 1140 Ma; Clark et al., 2000; Spaggiari et al., 2011). The tectonic setting for Stage I is uncertain, but recent work suggests an extensional rift or backarc setting, rather than collision, whereas Stage II is likely to have occurred in an intracratonic setting. Understanding the tectonic components that make up the Eucla basement is therefore crucial to constraining the Albany–Fraser Orogen's geodynamic history, and to answer the questions: where is the edge of the orogen, and what lies beyond?

The Rodona Shear Zone, a large, complex structure that may be truncated by the Mundrabilla Shear Zone to the

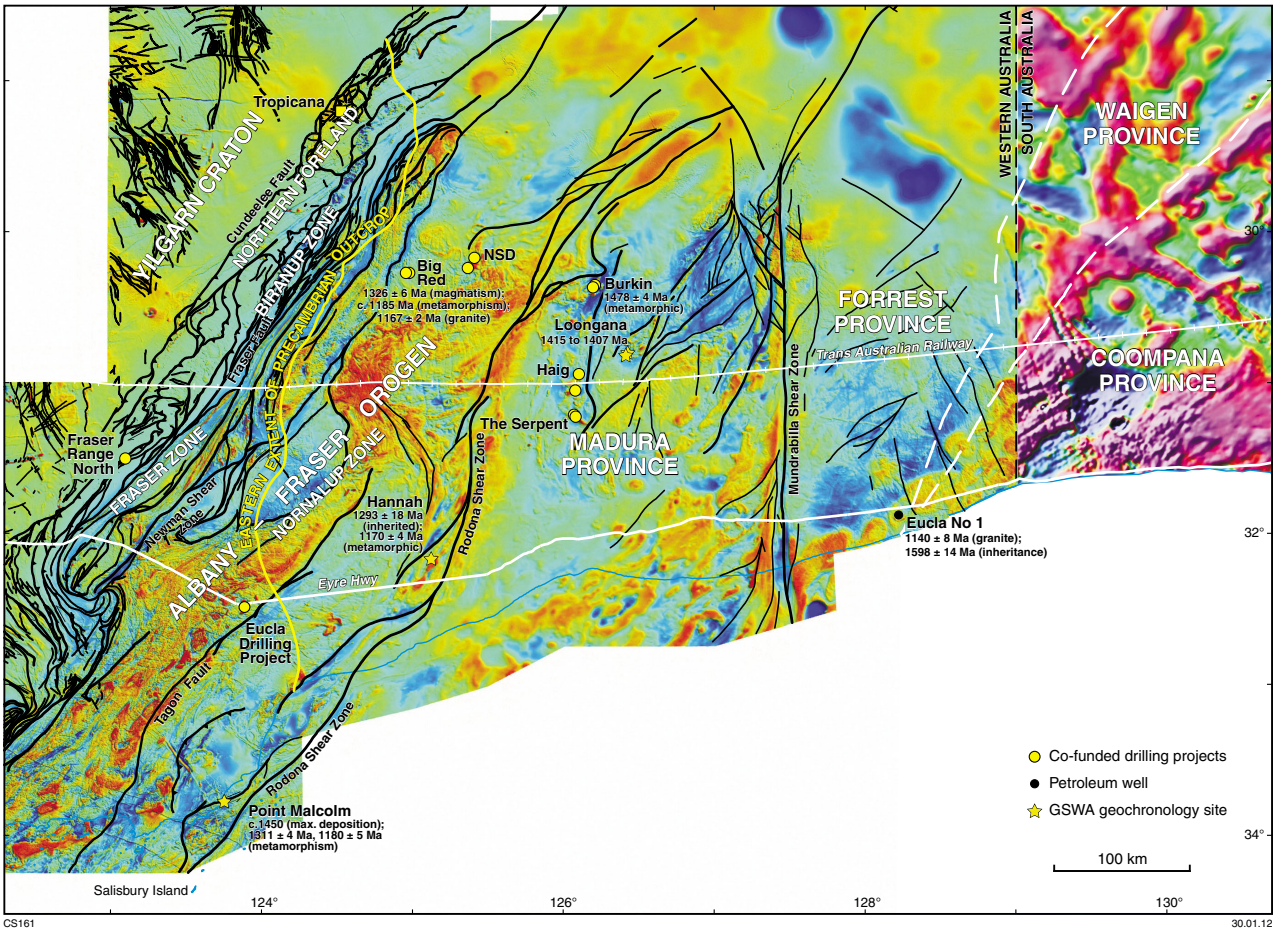

Figure 1. ***Reduced-to-pole aeromagnetic image, including preliminary data for Jubilee–Waigin–Mason (northeastern Eucla), over the eastern Albany–Fraser Orogen and Eucla Basin, showing major tectonic units and structures, and the locations of drilling and geochronology sites. The yellow line marks the approximate eastern outcrop limit of the Precambrian basement. Note that the Waigen Province should not be confused with the Waigen Sub-basin or Region of the Officer Basin, and the Madura Province is separate from the Madura Shelf of the Eucla Basin.***

northeast, is currently inferred to approximate the eastern edge of the eastern Nornalup Zone, and thereby the Albany–Fraser Orogen (Fig. 1). However, this is based on a small geochronology dataset that suggests differences in the ages of magmatic and metamorphic rocks on either side of the shear zone.

Madura Province

The Madura Province is defined as the area of basement bounded by the Rodona Shear Zone and the Mundrabilla Shear Zone (Fig. 1). The Mundrabilla Shear Zone is a prominent, north–south structure that abruptly loses its magnetic signature to the north under the Officer Basin. It is a wide, straight, shear zone, which suggests it is subvertical, with drag fabrics indicative of a sinistral shear sense, at least during its more recent history. The shear zone is coincident with a surface fault and present-day scarp through the Miocene limestones of the Eucla Basin. Other basement structures also cut these limestones, indicating that they were reactiviated. Aeromagnetic data indicate a complex structural architecture for the Madura Province, with a dominant northeasterly regional trend. So far, geochronology of drillcore samples from the Madura Province has yielded dates between c. 1480 and 1407 Ma, which are ages unlike those recorded in the Albany–Fraser Orogen, with exceptions being the detritus found in paragneiss from Point Malcolm in the eastern Nornalup Zone (Fig. 1; Adams, 2011), and in metasedimentary rocks of the Fraser Zone.

Exploration drilling in the Madura Province has intersected ultramafic, metagabbroic, and metagranitic rocks at the Loongana prospect; variably to strongly magnetic metagabbro at The Serpent prospect; and heterogeneous gneissic rocks, iron-rich layered quartz–chlorite–garnet schists, metamorphosed banded iron-formation, and amphibolite at the Burkin prospect (Fig. 1). Although not dated, it is possible that rocks of The Serpent prospect, which is defined by an elongate, northwesterly trending magnetic high (Fig. 1), may have formed during the same magmatic event as the nearby Loongana prospect. Granite, interpreted as either intrusive into, or

coeval with, metagabbro from the Loongana prospect (LNGD0002), yielded a date of 1415 ± 7 Ma (GSWA 178070*), interpreted as the igneous crystallization age of the granitic protolith. Nearby fine-grained, equigranular, unfoliated biotite microtonalite from LNGD0001 yielded a date of 1408 ± 7 Ma (GSWA 178071), also interpreted as the igneous crystallization age. The age of the microtonalite is identical to the igneous crystallization age of 1407 ± 7 Ma obtained for medium- to coarse-grained, foliated biotite tonalite gneiss taken from the same core (GSWA 178072). Lutetium–hafnium data from the dated samples are consistent with mixed sources, including juvenile mantle and unradiogenic Archean material. This implies mantle input into the crust during the magmatic event at c. 1410 Ma. It is interesting to note that the juvenile lutetium–hafnium signature seen in the Loongana samples is similar to that of c. 1400 Ma detritus found in the c. 1300 Ma Fraser Range Metamorphics, suggesting that this detritus may have been derived from Loongana or related rocks.

Migmatitic gneiss from the Burkin prospect (GSWA 182485) yields a date of 1478 ± 4 Ma, interpreted as the age of migmatization and high-grade metamorphism. This indicates an older protolith than for the Loongana prospect, and an older metamorphic event. Leucosomes in the dated sample crosscut a folded fabric, indicating deformation prior to migmatization. Three zircon cores yielded dates of 2408–2293 Ma, which could be interpreted as the age of detritus, provided the gneiss has a sedimentary protolith. Four other zircon cores yielded a mean date of 1538 ± 17 Ma, which could represent a maximum depositional age.

The presence of younger metasedimentary rocks in the Madura Province is indicated by the Salisbury Gneiss, exposed on Salisbury Island southeast of Esperance and east of the Rodona Shear Zone (Fig. 1). The Salisbury Gneiss comprises pelitic gneiss, mafic granulite, porphyritic granitic gneiss, and two-pyroxene metagabbro (Clark et al., 2000). Migmatitic pelitic gneiss records granulite-facies conditions of approximately 800°C and >5 kbar (Clark et al., 2000). The depositional age of the pelitic gneiss' protolith is unknown, although a migmatitic leucosome yielded dates of 1214 ± 8 and 1182 ± 13 Ma, consistent with the range of metamorphic ages of Stage II of the Albany–Fraser Orogeny. The older date is interpreted as the crystallization age of the leucosome, whereas the younger date is interpreted as the age of decompression from peak metamorphic conditions (Clark et al., 2000).

Forrest Province

The Forrest Province is defined as the basement east of the Mundrabilla Shear Zone, but no obvious structure defines its eastern contact with the Waigen Province in Western Australia (Fig. 1). As with the Madura Province, aeromagnetic data indicate a complex structural architecture, and a dominant northeasterly regional trend that appears to be truncated by northwesterly trending structures. The latter structures also cut a series of interpreted, moderately to strongly magnetic granitic intrusions, which form a series of northeasterly trending plutons near the coast that continue into South Australia (Fig. 1).

The Eucla 1 petroleum well intersected one of these plutons — a distinct ovoid feature with high magnetic intensity (Fig. 1). Small rock chips from the base of the well, which are interpreted as derived from a granitic rock, contain oscillatory zoned zircons that yielded a date of 1140 ± 8 Ma, interpreted as the magmatic crystallization age of the granite (GSWA 194773). A single analysis of an unzoned zircon yielded a date of 1598 ± 14 Ma, interpreted as either the age of an inherited component within the granite, or the age of zircon incorporated from another rock unit (e.g. sedimentary rock) within the drillhole. The magnetic signature, together with the c. 1140 Ma age, of these rocks suggests that the intrusion is related to the Esperance Supersuite of the Albany–Fraser Orogen. Similar plutons are inferred in the Madura Province, suggesting a common link from the Albany–Fraser Orogen to as far east as the Forrest Province by at least this time. The plutons are cut by the Mundrabilla Shear Zone, indicating that at least one phase of movement on the structure post-dates these intrusions.

References

Adams, M 2011, Structural and geochronological evolution of the Malcolm Gneiss, Nornalup Zone, Albany–Fraser Orogen, Western Australia: Curtin University, Perth, Western Australia, BSc (Honours) thesis (unpublished).

Clark, DJ, Hensen, BJ and Kinny, PD 2000, Geochronological constraints for a two-stage history of the Albany–Fraser Orogen, Western Australia: Precambrian Research, v. 102, no. 3, p. 155–183.

Kirkland, CL, Spaggiari, CV, Pawley, MJ, Wingate, MTD, Smithies, RH, Howard, HM, Tyler, IM, Belousova, EA and Poujol, M 2011, On the edge: U–Pb, Lu–Hf, and Sm–Nd data suggests reworking of the Yilgarn Craton margin during formation of the Albany–Fraser Orogen: Precambrian Research, v. 187, p. 223–247.

Shaw, RD, Wellman, P, Gunn, P, Whitaker, AJ, Tarlowski, C and Morse, M 1996, Guide to using the Australian Crustal Elements Map: Australian Geological Survey Organisation, Record 1996/30, 44p.

Spaggiari, CV, Kirkland, CL, Pawley, MJ, Smithies, RH, Wingate, MTD, Doyle, MG, Blenkinsop, TG, Clark, C, Oorschot, CW, Fox, LJ and Savage, J 2011, The geology of the east Albany–Fraser Orogen — a field guide: Geological Survey of Western Australia, Record 2011/23, 98p.

Wade, BP, Payne, JL, Hand, M and Barovich, KM 2007, Petrogenesis of ca 1.50 Ga granitic gneiss of the Coompana Block: filling the 'magmatic gap' of Mesoproterozoic Australia: Australian Journal of Earth Sciences, v. 54, p. 1089–1102.

* GSWA geochronology reports are available online at <www.dmp.wa.gov.au/geochron/>.

The importance of lithogeochemistry to the west Musgrave Province mapping project

by

RH Smithies, HM Howard, and CL Kirkland

The Musgrave Province lies at the intersection of central Australia's Proterozoic structural trends, and chronicles a long and complex history of high-grade metamorphism, deformation, and magmatism. Although the region contains significant nickel–copper sulfide and nickel laterite mineralization, the Musgrave Province has remained very much 'greenfields' in terms of its economic mineral endowment and geological understanding. Early work in the area (e.g. Daniels, 1974; Gray, 1971; White, 1997) established a broad lithological and geochronological framework, and Glikson et al. (1996) provided a more detailed lithological and mineralogical background for the mafic–ultramafic Giles intrusions. However, there is a lack of clear understanding of the geological and tectonic context of the Giles intrusions, and broader insight into the geological evolution of the province in general is also lacking.

Since the the west Musgrave Province mapping project commenced in 2004, geological understanding of this region has increased significantly, and views on its geological evolution have changed markedly. A large part of this advance can be directly attributed to the collection and interpretation of large, high-quality lithogeochemical and geochronological datasets. The usefulness of such datasets depends on the ability to successfully characterize real lithological groups, which in turn depends directly on the quality and amount of data collected. The full value of lithogeochemical datasets as both a mapping tool, and as an aid to deciphering the geological history of a region and its deep crustal architecture, cannot be overstated. Examples of how these datasets have contributed to the west Musgrave Province mapping project are given below.

Lessons from the lithogeochemistry

As for many Proterozoic terranes, distinguishing between various generations of mineralogically similar igneous rocks in the field is greatly hindered by general similarities in primary texture, and by locally intense deformational overprints. In the west Musgrave Province, this is particularly the case for the granites, but is also true of the complex magmatic assemblages formed during the 1085–1040 Ma Giles Event.

Granites

Granites, of all ages, regionally dominate outcrop in the west Musgrave Province, and most are virtually indistinguishable feldspar porphyritic monzogranites and syenogranites. Previous regional mapping projects generally failed to provide any reliable basis for subdivision of these rocks, and the prevailing view was that the overwhelming majority formed during the c. 1200 Ma Musgrave Orogeny. However, using a dataset of >1300 high-quality lithogeochemical analyses, all Musgrave granites can now be assigned to one of four compositionally and geochronologically constrained supersuites (Figs 1 and 2), which includes voluminous felsic magmatism both significantly older and younger than the Musgrave Orogeny. These supersuites are:

- The c. 1400 Ma Papulankutja Supersuite and 1345–1293 Ma Wankanki Supersuite, which are mainly concentrated within the central and southern parts of the west Musgrave Province. Both supersuites are of calc-alkaline affinity, formed through the dehydration melting of c. 1900 Ma juvenile crust, most likely in a continental-arc setting.
- The 1220–1150 Ma Pitjantjatjara Supersuite of ferroan, alkali-calcic granites, concentrated in the central and northeastern parts of the west Musgrave Province. These rocks formed through the melting of a source that homogenized c. 1900 Ma juvenile crust into mantle-derived melts in an intracratonic setting.
- The 1085–1040 Ma Warakurna Supersuite of ferroan, alkali-calcic granites and rhyolites, found throughout all but the far northeast of the west Musgrave Province. These rocks formed during the Giles Event as partial-melts of crust incorporated into mantle-derived melts in an intracontinental rift setting.

These granites can now be directly assigned to specific orogenic events, source regions, and tectonic settings, and their geographic extent can be mapped. Combining this information with detailed petrogenetic constraints imposed by the geochemistry of the individual supersuites and component suites allows us to establish a detailed tectonic history for these rocks. For example, the geochemistry of the Pitjantjatjara Supersuite generally indicates unusually

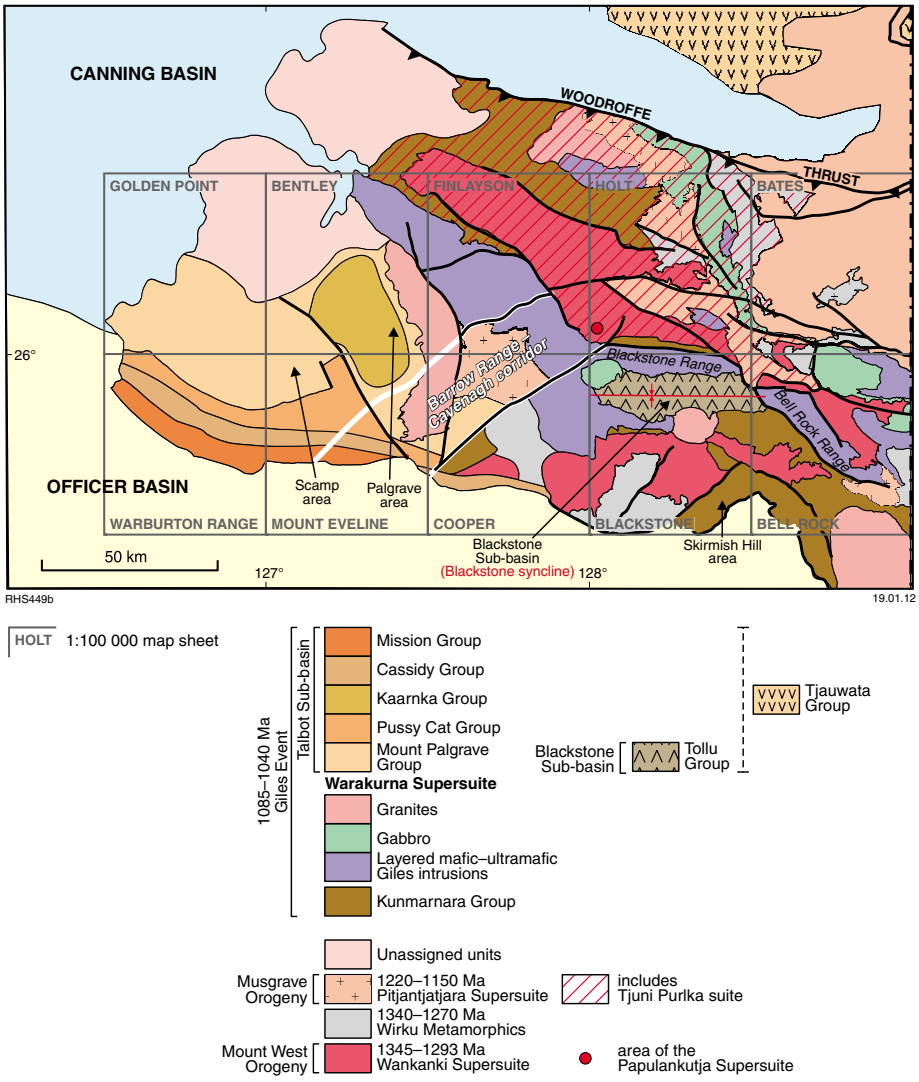

Figure 1. Regional sketch of the west Musgrave Province and Bentley Basin.

high-temperature (>1000°C) magmatism. Within this supersuite, the Tjuni Purlka suite is geochemically unique, and is restricted to a strongly tectonized northwest-trending zone in the central part of the west Musgrave Province, which can then be inferred to be a crustal-scale feature that channelled lower-crustal magmas during the Musgrave Orogeny. A change from ytterbium-depleted to ytterbium-undepleted granite compositions in the early stages of the Musgrave Orogeny reflects both a switch from deep crustal melting to much shallower crustal melting, and a likely change in lower crustal architecture, with this change occurring at slightly different times across major structures. Furthermore, the antithetic distribution of the Wankanki and Pitjantjatjara Supersuites provides information on the changing lower crustal architecture between the c. 1300 Ma Mount West Orogeny and the c. 1200 Ma Musgrave Orogeny, and on the distribution of fertile sources or heat (or both) at depth during the Musgrave Orogeny.

Igneous rocks of the Giles Event

Intrusive and extrusive rocks of the Giles Event (Warakurna Supersuite) outcrop over approximately half of the west Musgrave Province (Fig. 1). These rocks comprise a bimodal suite with mafic and felsic components produced throughout virtually the entire 45 m.y. duration of the event.

The mafic dykes, sills, layered intrusions, and flows form at least ten different units, with the giant, layered Giles intrusions being the most extensive. Each of these mafic units has geochemical attributes that permit unique identification; again, the key here is in collecting enough data to uniquely define these attributes. Of particular interest is the Alcurra Dolerite, a c. 1067 Ma regionally distributed suite that hosts nickel–copper sulfide mineralization at Nebo–Babel, and is associated with copper mineralization elsewhere in the region.

The magmatic conduits for several of these mafic units were major crustal-scale structures active at the time of magmatism (magmatic shear zones).

Likewise, felsic dykes, sills, plutons, and volcanic rocks of the Giles Event form at least 17 different units — each with unique geochemical attributes (Fig. 3). Units in the eastern and northern parts of the region (on Blackstone, Bell Rock, Holt, Finlayson, and the eastern part of the Cooper map sheet — including units in the Blackstone Sub-basin) are generally older (1078–1068 Ma) and are, as a group, compositionally distinct from units to the south and west (on the Mount Eveline, Bentley, Warburton Range, and Golden Point map sheets — including units in the Talbot Sub-basin). This implies two regions with distinct mantle and/or crustal source components. The exception to this is the Alcurra Dolerite (which includes fractionated trachydacitic equivalents), which is found in both regions. The boundary between the two regions is the northeast-trending Barrow Range – Cavenagh corridor (Fig. 1). This structural corridor reflects a mantle-tapping, crustal-scale feature, into which the hosts of the Nebo–Babel nickel–copper sulfide mineralization were emplaced.

The volcanic units of the Warakurna Supersuite in the northeastern Talbot Sub-basin provide a particular challenge to mapping, as all felsic units are similar looking, glassy rhyolitic rocks. However, individual units are compositionally distinct (Fig. 3), and this difference has allowed the construction of a robust stratigraphic section significantly different to previous interpretations.

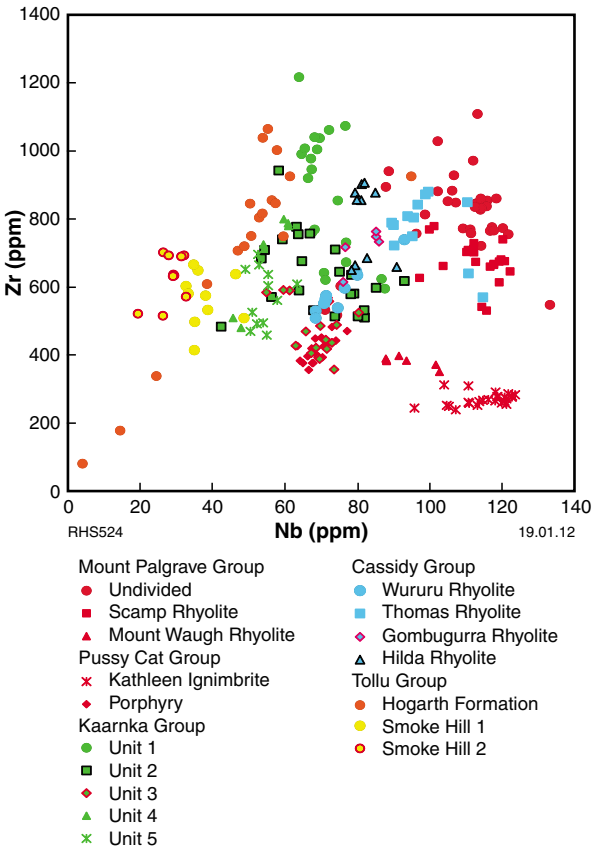

Figure 3. Compositional variation diagram for felsic volcanic rocks of the Warakurna Supersuite, plotting zirconium vs niobium.

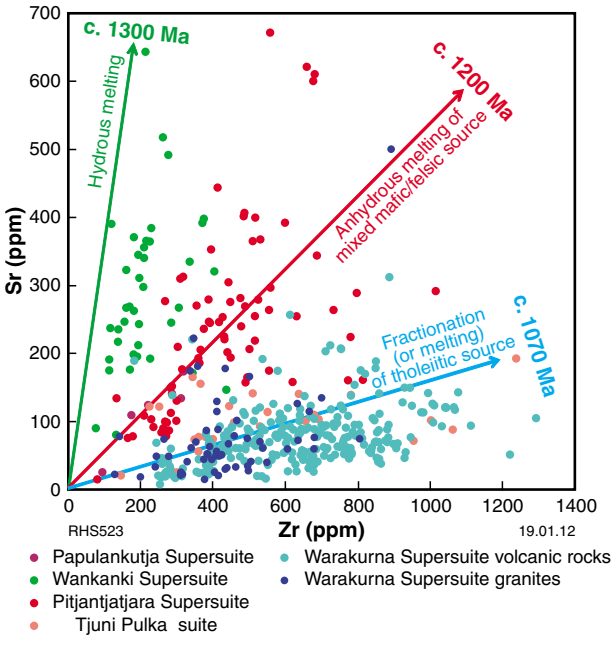

Figure 2. Compositional variation diagram for granites of the west Musgrave Province, plotting strontium vs zirconium for the four supersuites, and the felsic volcanic rocks of the Warakurna Supersuite. The arrows give a petrogenetic interpretation of the various trends. Using a combination of this and similar variation diagrams, virtually all granites of the region can be confidently grouped.

This in turn has altered the interpreted geological history for this unit; for example, the Scamp and Palgrave areas (Fig. 1) have now been combined into a regionally developed basal group (Mount Palgrave Group) of the Talbot Sub-basin, instead of representing two lithologically and chronologically independent calderas. However, the Mount Palgrave Group is overlain by the more geographically restricted Kaarnka Group, which may define a caldera.

References

Daniels, JL 1974, The geology of the Blackstone region, Western Australia: Geological Survey of Western Australia, Bulletin 123, 257p.

Glikson, AY, Stewart, AT, Ballhaus, GL, Clarke, GL, Feeken, EHT, Level, JH, Sheraton, JW and Sun, S-S 1996, Geology of the western Musgrave Block, central Australia, with reference to the mafic–ultramafic Giles Complex: Australian Geological Survey Organisation, Bulletin 239, 206p.

Gray, CM 1971, Strontium isotope studies on granulites: Australian National University, Canberra, Australian Capital Territory, PhD thesis (unpublished), 242p.

White, RW 1997, The pressure–temperature evolution of a granulite facies terrain, western Musgrave Block, central Australia: Macquarie University, Sydney, New South Wales, PhD thesis (unpublished), 256p.

ROYALTIES FOR REGIONS
EXPLORATION INCENTIVE SCHEME

A multi-isotopic approach to the crustal evolution of the west Musgrave Province

by

CL Kirkland, RH Smithies, A Woodhouse[1], MTD Wingate, HM Howard, J Cliff[2], and EA Belousova[3]

The timing and mechanism of crust formation are both important factors in understanding the mineral wealth of a region, as juvenile addition from the mantle into the crust directly or indirectly controls the mineral endowment. Hafnium and neodymium isotopic evolution can constrain the timing of crust formation, provided that the recorded isotopic signal is not a mixture between materials formed at different times.

The Mesoproterozoic Musgrave Province of central Australia possibly represents one of the most extreme cases of an extension-related, high field strength element (HFSE)-enriched, magmatic province. This enrichment has had a profound influence on the evolution patterns for isotopes of HFSE (e.g. hafnium and neodymium), which warrants special consideration. Known magmatism in this region extends from c. 1400 to c. 1040 Ma, and is characterized by four major magmatic events, of which at least two were intracratonic (Smithies et al., 2010; Smithies et al., 2011). Although the nature of basement to the province is cryptic, the neodymium and hafnium isotopic evolution of nearly all rocks in the Musgrave Province requires the presence of a Paleoproterozoic to early Mesoproterozoic juvenile basement with a minor Archean component (Smithies et al., 2010; Wade et al., 2006). The oldest exposed rocks in the west Musgrave Province was previously thought to be the calc-alkaline igneous rocks of the 1345–1293 Ma Wankanki Supersuite, interleaved with near-contemporaneous paragneisses of the Wirku Metamorphics; however, new geochronology has revealed the presence of exposed 1402 ± 4 Ma crystalline rocks of the Papulankutja Supersuite (Howard et al., 2011). The Papulankutja Supersuite defines the earliest component of the isotopic dataset that constrains crust formation within the Musgrave Province.

1 Continental Evolution Research Group, The University of Adelaide, Adelaide SA 5005

2 The Centre for Microscopy, Characterisation and Analysis, The University of Western Australia, Crawley WA 6009

3 GEMOC, Department. of Earth and Planetary Sciences, Macquarie University, Sydney NSW 2109

Isotopic constraints on crust formation

Neodymium and hafnium isotopic model ages and evolution diagrams, from magmatic rocks and sediments throughout the Musgrave Province, indicate a major juvenile-crust formation event at 1950–1900 Ma (Fig. 1). Although there are no physical remnants of this 1950–1900 Ma juvenile material, contemporaneous radiogenic addition into the crust at this time is required to account for the consistent hafnium and neodymium isotopic evolution patterns in rocks that sourced this material. Furthermore, the correspondence between this mantle extraction age and the time at which reworking of Archean material commenced strongly indicates that these ages reflect a real 1950–1900 Ma crust-formation event. The general trend of hafnium and neodymium isotopic evolution apparently implies reworking of a dominant 1950–1900 Ma source, with only minor additional unradiogenic and radiogenic input through time. However, the crust had become so HFSE-enriched during the prolonged intracontinental Musgrave Orogeny (1220–1150 Ma) that it was insensitive to later inputs of mantle material, which had very low concentrations of hafnium and neodymium. This makes the addition of juvenile material during and after the Musgrave Orogeny difficult to distinguish from crustal reworking isotopic trends. Although the Musgrave Province is an extreme case of a HFSE-enriched magmatic province, it is possible that considerable amounts of juvenile input have gone undetected in isotopic data in other intracratonic orogens; as a corollary, estimates of the amount of juvenile crustal growth in intracratonic extensional settings may also have been underestimated.

Oxygen isotopes from zircons in magmas incorporating near-surface rocks (those with $\delta^{18}O_{SMOW} > 6.3$ ‰) are likely to yield mixed model ages; these model ages are unlikely to represent discrete crust-forming events (Hawkesworth and Kemp, 2006). Zircons in equilibrium with mantle-derived melts will have $\delta^{18}O_{SMOW}$ values of 5.3 ± 0.6 ‰, and will more likely yield model ages that reflect juvenile crust formation (Valley, 2003). The $\delta^{18}O$ values from Papulankutja Supersuite gneisses indicate that the most uncontaminated melts have model ages of 1950–1900 Ma, consistent with model ages reflecting crust

generation (Fig. 2). The oldest model ages generally have the most elevated $\delta^{18}O$ components, and are consistent with unradiogenic sediment incorporation into those magmas.

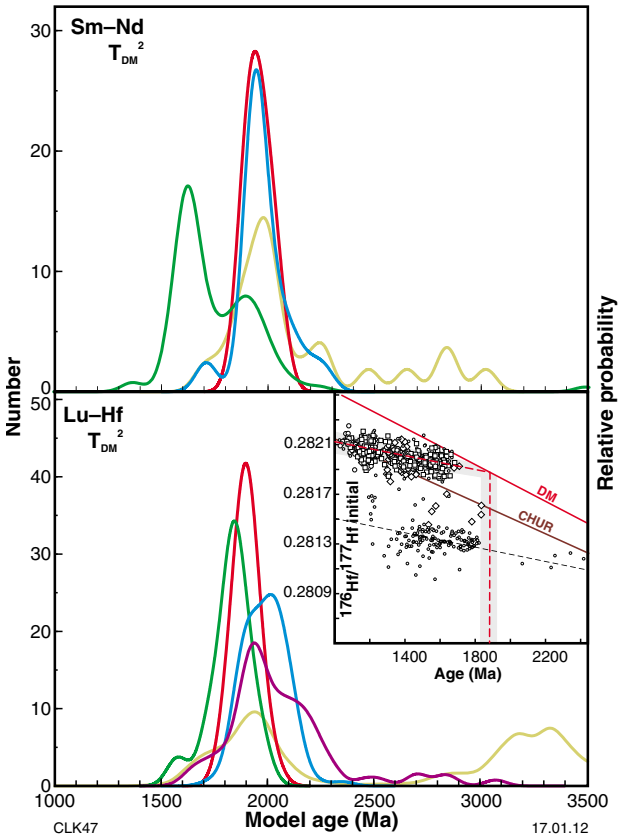

Figure 1. ***Probability density diagrams of model ages from the west Musgrave Province (top: samarium–neodynium whole-rock, bottom: lutetium–hafnium zircon). The y-axis records the number of data points contributing to the probability curve. Curve colours used: blue = Pitjantjatjara Supersuite; red = Wankanki Supersuite; green = Warakurna Supersuite; yellow = Wirku Metamorphics; purple = Papulankutja Supersuite. Inset chart shows an initial $^{176}Hf/^{177}Hf$ evolution diagram, with the hypothesized crust-formation event indicated by the red dashed line at c. 1900 Ma.***

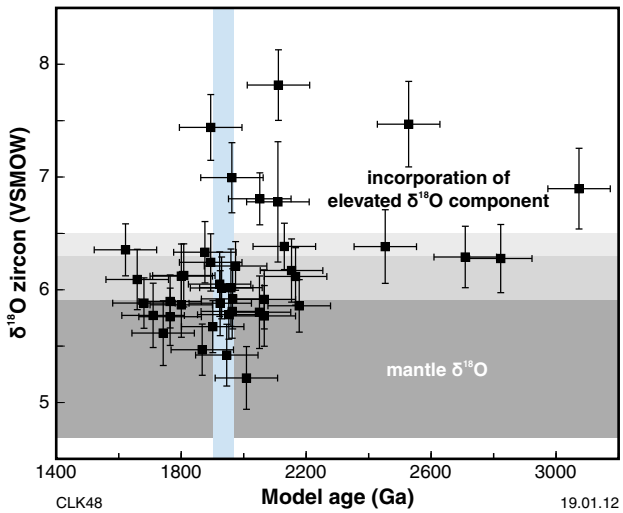

Figure 2. ***Zircon $\delta^{18}O$ (VSMOW) versus hafnium crustal model ages from the same zircon crystals. Vertical bar indicates time of hypothesized crust-formation event. Values within grey horizontal bars indicate zircon with minimal (<6.3 per mil) and no influence of crustal material. Note the generally higher $\delta^{18}O$ values for zircon grains with model ages >1950 Ma.***

Implications for crustal evolution of the west Musgrave Province

The Papulankutja Supersuite comprises c. 1400 Ma calc-alkaline granodioritic and monzogranitic basement rocks. Neodymium and hafnium data from this exposed basement, and its derivative products, imply an isotopically homogeneous juvenile source with a mafic to intermediate bulk composition, isolated from the mantle at 1950–1900 Ma. This source dominates the subsequent isotopic evolution of the province through apparent recycling events at c. 1400, 1345–1293, 1220–1150, and 1085–1040 Ma. Although the hafnium and neodymium isotope arrays for the Musgrave Province are dominated by apparent recycling trends, the range of geological data requires significant mantle contribution associated with the 1220–1150 Ma Musgrave Orogeny and the 1085– 1040 Ma Giles Event. Both of these younger magmatic events coincide with marked changes in felsic magma composition, towards an extreme enrichment in HFSE.

Reworking of an Archean source was near-synchronous with the formation of the 1950–1900 Ma mafic to intermediate basement. In addition, neither the 1950–1900 Ma juvenile crust, nor a subsequent 1650–1550 Ma juvenile component identified in the Musgrave Province basement, provide any evidence of a direct link between the province and the currently proximal Proterozoic terranes to the north (the Arunta, and specifically, the Warumpi Province) and southwest (Albany–Fraser Orogen) before c. 1400 Ma. Hence, the Musgrave Province likely formed in isolation from the southern margin of the North Australian Craton. It is possible that the 1950–1900 Ma basement developed as an active margin underplate, at or near the Archean Gawler Craton to the south.

References

Hawkesworth, CJ and Kemp, AIS 2006, The differentiation and rates of generation of the continental crust: Chemical Geology, v. 226, no. 3–4, p. 134–143, DOI: http://dx.doi.org/10.1016/j.chemgeo.2005.09.017.

Howard, HM, Werner, M, Smithies, RH, Evins, PM, Kirkland, CL, Kelsey, DE, Hand, M, Collins, AS, Pirajno, F, Wingate, MTD, Maier, WD and Raimondo, T 2011, The geology of the west Musgrave Province and the Bentley Supergroup — a field guide: Geological Survey of Western Australia, Record 2011/4, 116p.

Smithies, RH, Howard, HM, Evins, PM, Kirkland, CL, Kelsey, DE, Hand, M, Wingate, MTD, Collins, AS, Belousova, E and Allchurch, S 2010, Geochemistry, geochronology, and petrogenesis of Mesoproterozoic felsic rocks in the west Musgrave Province, Central Australia, and implications for the Mesoproterozoic tectonic evolution of the region: Geological Survey of Western Australia, Report 106, 73p.

Smithies, RH, Howard, HM, Evins, PM, Kirkland, CL, Kelsey, DE, Hand, M, Wingate, MTD, Collins, AS and Belousova, E 2011, High-temperature granite magmatism, crust–mantle interaction and the Mesoproterozoic intracontinental evolution of the Musgrave Province, Central Australia: Journal of Petrology, v. 52, p. 931–958.

Valley, JW 2003, Oxygen isotopes in zircon: Reviews in Mineralogy and Geochemistry, v. 53, p. 343–385, doi:10.2113/0530327.

Wade, BP, Barovich, KM, Hand, M, Scrimgeour, IR and Close, DF 2006, Evidence for early Mesoproterozoic arc magmatism in the Musgrave Block, Central Australia: implications for Proterozoic crustal growth and tectonic reconstructions of Australia: Journal of Geology, v. 114, p. 43–63.

ROYALTIES FOR REGIONS
EXPLORATION INCENTIVE SCHEME

Multiscale dynamics of orebody formation

by

B Hobbs[1], W Gorczyk[1], A Ord[1], and K Gessner[1]

The formation of large orebodies involves interlinked chemical and physical processes that operate from the nano to the lithospheric scale. In general, it is not possible to consider all these scales simultaneously to the same level of detail, so the processes that operate at one particular scale are often grouped or averaged to provide a basis for the next scale up. Equally, if one wants to understand what is happening at one particular scale, the physical conditions that operate at the next scale up can act as boundary conditions or constraints on what happens at the next scale down. We refer to this as a multiscale approach, and it results in an integrated, holistic approach to ore system analysis (Fig. 1). This project is an ARC Linkage project with funding from the GSWA, PIRSA (now DIMITRE), and the Silver Swan Group. The aim is to establish measurable parameters and indices that enable researchers to identify the differences between 'successful' and 'failed' hydrothermal systems from outcrops or drillcore, and to identify vectors to mineralization within 'successful' systems. This approach has led us to the conclusion that mineralizing systems operate far from equilibrium, and in fact never reach equilibrium (Ord et al., in press).

Here we concentrate on the lithospheric scale of an orebody, but also consider the outcrop and mine scales. The lithospheric-scale investigations are based on the observation that many large hydrothermal systems have their origins in intracratonic settings, far removed from any subduction zones. There are, of course, an important group of mineralizing systems associated directly with subduction zones, but these are not considered as part of this project. Examples of mineralized hydrothermal systems in intracratonic settings include the Olympic Dam iron oxide – copper – gold, Yilgarn orogenic gold, Carlin gold, and, arguably, the Mount Isa systems. Similar examples may emerge from the as yet unprospective Arunta Orogen and Musgrave Province.

For the moment, we are exploring the proposition (based largely on the work of Begg et al., 2009) that these mineral systems form within intracratonic orogens, coincident with zones of metasomatism in the subcontinental lithospheric mantle (SCLM) that have been reactivated at the time of mineralization. We show that tectonic deformation can cause spontaneous delamination of the SCLM in these zones, causing a concurrent and subsequent history of deformation, fluid infiltration from various depths within the SCLM, melting, and metamorphism, accompanied by surface processes such as erosion and sedimentation, all of which can last for 100 m.y. after a relatively rapid delamination. All of these processes leave their marks in the geological record, and can be indicative of an active mineralizing system (Gorczyk et al., 2012). Low-salinity fluids from relatively shallow depths, and CO_2-rich fluids from deep in the previously metasomatized SCLM are both involved. The delamination process is a new kind of Rayleigh–Taylor instability that forms in solids, rather than the classical Rayleigh–Taylor instability studied in viscous fluids by Houseman and Molnar (1997) and Elkins-Tanton (2007; see also Huismans and Beaumont, 2002). Delamination of the SCLM causes a thermal–mechanical disturbance producing types of deformation, metamorphism, melting, and fluid flow at least comparable with that produced at subducting margins. Such delamination events are being imaged increasingly in modern, or relatively recently mineralized, intracratonic settings (West et al., 2009; Guoming et al., 2011).

Recent results from the Albany–Fraser Orogen (Spaggiari et al., 2011) and the Western Australian part of the Musgrave Province (Howard et al., 2011; Smithies et al., 2012) provide tectono-thermal histories for these two regions; these data are summarized in Tables 1 and 2. The timescales associated with the tectono-thermal histories of these two regions are important. Since a thermal pulse diffuses (by conduction) through a rock thickness L (in metres), on a timescale given by 10^6L^2 (in seconds), timescales of 570 m.y. and 305 m.y. correspond to rock thicknesses of 135 km and 100 km, respectively, which are equivalent to lithospheric thicknesses. Conversely, the individual events lasting 100 m.y. and 40 m.y. are thermal events corresponding to rock thicknesses of 56 km and 35 km, respectively, corresponding to viable crustal thicknesses. The delamination process involves relatively rapid solid advection of SCLM through isotherms, and slow post-delamination tectonic relaxation. Thus, the timescales of 100 m.y. or less shown in Tables 1 and 2 can be explained by the delamination process, as

1 Centre for Exploration Targeting, The University of Western Australia, Stirling Highway, Nedlands WA 6009

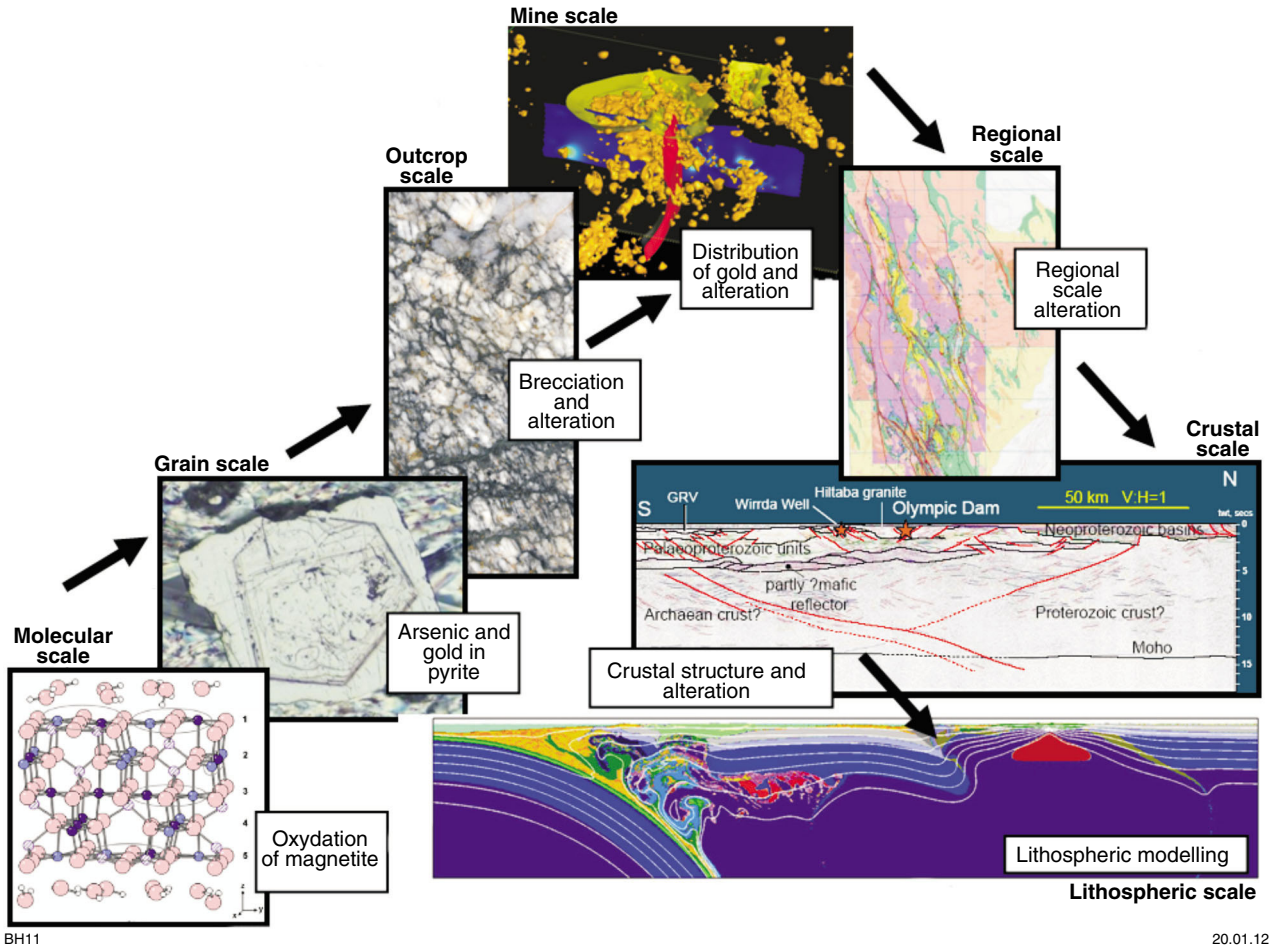

Figure 1. A multiscale approach to hydrothermal mineralizing systems

a result of which (at least) crustal material remains at high temperatures and pressures for extended periods corresponding to the post-delamination thermal relaxation.

Just as important as the tectono-thermal timescales is the width of the SCLM weak zone as an influence on patterns of deformation, melting, and fluid release that result during delamination (Fig. 4). After a critical width is exceeded, the pattern of deformation becomes localized, forming Y-shaped fault structures within the crust. The SCLM is advected into higher pressure–temperature regions below this structure, resulting in localized melting and devolatilization. We propose that the development of this localized deformation to one side of the delamination system is the primary focusing mechanism for large hydrothermal orebodies, and as such, the width of the delamination system is a prime criterion for failed-versus-successful mineralizing systems. Note that this asymmetry is reflected in the evolution of surface topography, so there will be a direct record in the stratigraphic history. This can be seen in the Albany–Fraser Orogen and Musgrave Province.

At the orebody scale, it is important to treat the development of these hydrothermal systems as open-flow chemical reactors (Ord et al., in press). Here, constraints imposed by the lithospheric-scale modelling presented above can be used to impose time and volumetric flow-rate constraints on the evolution of the system. This analysis results in a common history for all successful hydrothermal systems involving an initial stage of exothermic alteration (hydrous minerals, carbonates, and iron oxides) and the following endothermic precipitation of sulfides, metals, and silicates. The switch from one mode of operation to another requires a new mechanism for maintaining permeability, and this is commonly expressed as a stage (or several stages) of brecciation or vein formation. Also at this switch from one mode of operation to another, the most efficient systems must be localized, and this is seen as zoned mineralization or late stage alteration.

This non-equilibrium approach supplies several criteria for deciding whether a particular mineralizing system has been successful or not, based on drillcore or exposures.

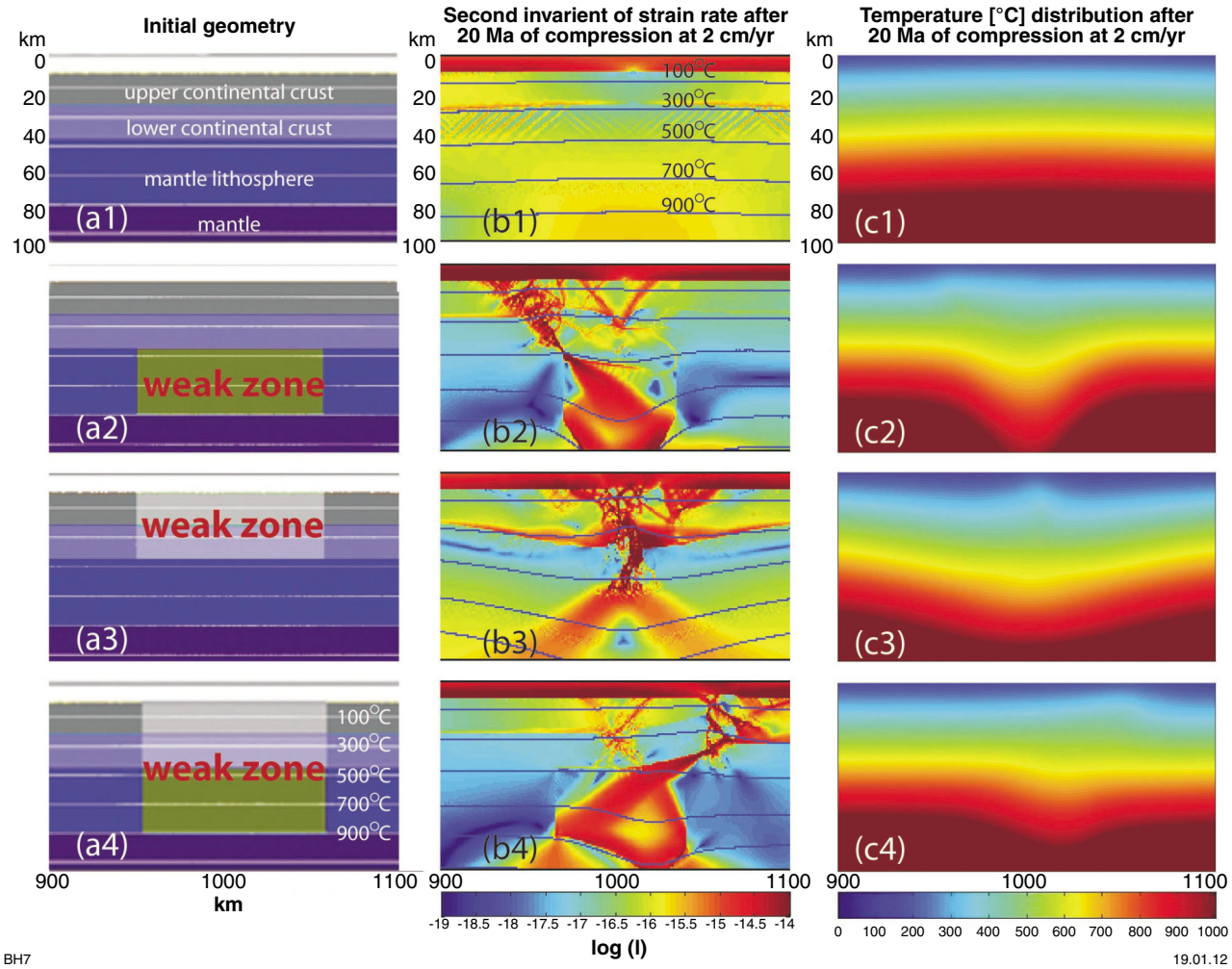

Figure 2. Results of four models with different initial geometries, showing: (a) initial geometry and bulk composition; (b) second strain rate invariant after 20 Ma of compression at rate of 2 cm/a; (c) temperature distribution after period of 20 Ma (from Gorczyk et al. 2012).

Table 1. Albany–Fraser tectonic regime

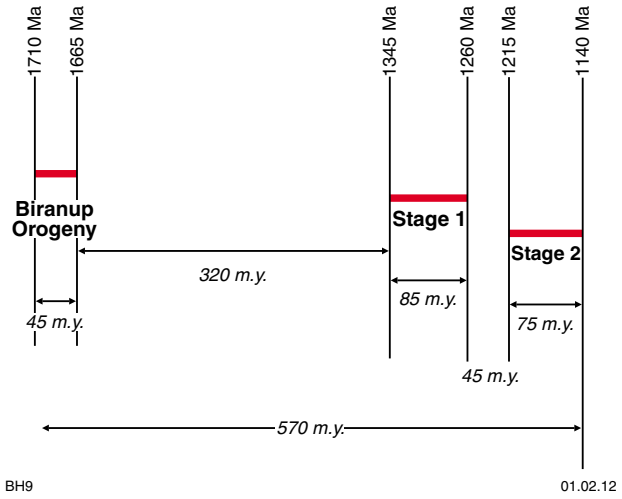

Table 2. Musgrave tectonic regime

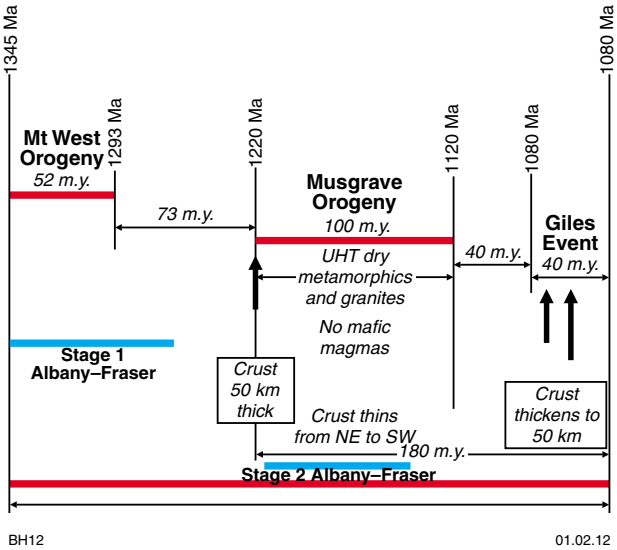

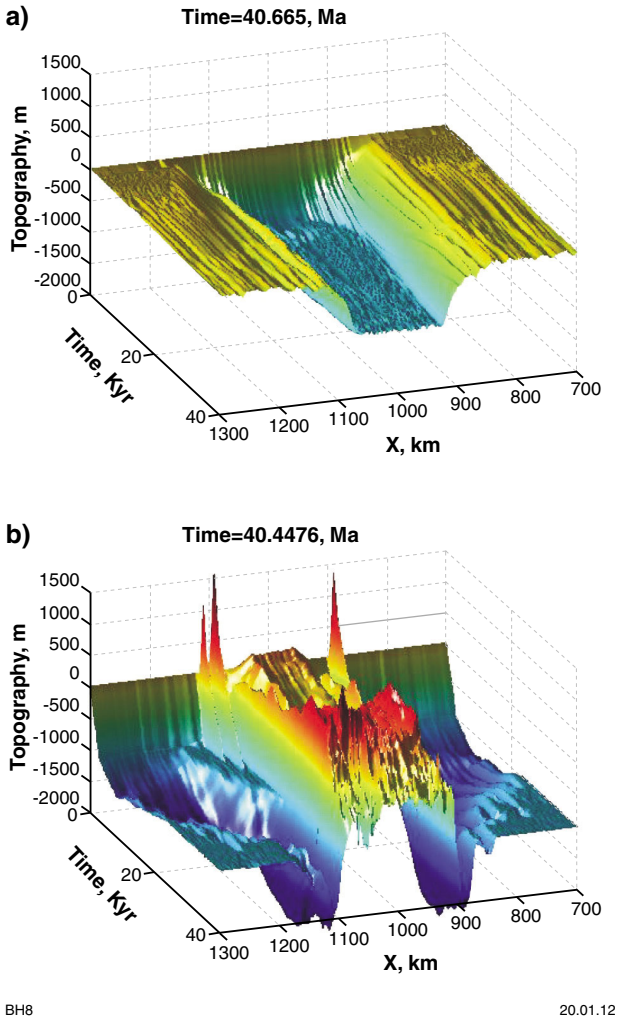

Figure 3. ***Dynamic evolution of the topography above the developing instability: (a) run with initial perturbation imposed only on mantle lithosphere; (b) run with initial perturbation imposed on whole lithosphere, with additional continental root. The initial peaks in topography on the sides of instability are due to the initial equilibration of topography. Further in the run, peaks above the downwelling correspond to intrusion of magma into the crust, plus mountain building processes, as a result of deep lithospheric detachment (from Gorczyk et al., 2012).***

References

Begg, GC, Griffin, WL, Natapov, LM, O'Reilly, SY, Grand, SP, O'Neill, CJ, Hronsky, JMA, Poudjom Djomani, Y, Swain, CJ, Deen, T and Bowden, P 2009, The lithospheric architecture of Africa: seismic tomography, mantle petrology, and tectonic evolution: Geosphere, v. 5, p. 23–50.

Elkins-Tanton, LT 2007, Continental magmatism, volatile recycling, and a heterogeneous mantle caused by lithospheric gravitational instabilities: Journal of Geophysical Research — Solid Earth, v. 112, B03405, doi:10.1029/2005JB004072.

Gorczyk, W, Hobbs, B and Gerya, T 2012, Initiation of Rayleigh–Taylor instabilities in intra-cratonic settings: Tectonophysics, v. 514–517, p. 146–155.

Guoming, J, Guibin, Z, Qingtian, L and Danian, S 2011, Seismic evidence of upwelling of mantle materials beneath the middle and lower Yangtze region: Proceedings of the international symposium on deep exploration into the lithosphere. Beijing, China, 16–18 November 2011, p. 44.

Houseman, GA and Molnar, P 1997, Gravitational (Rayleigh–Taylor) instability of a layer with non-linear viscosity and convective thinning of continental lithosphere: Geophysical Journal International, v. 128, p. 125–150.

Howard, HM, Werner, M, Smithies, RH, Kirkland, CL, Kelsey, DE, Hand, M, Collins, A, Pirajno, F, Wingate, MTD, Maier, WD and Raimondo, T 2011, The geology of the west Musgrave Province and the Bentley Supergroup — a field guide: Geological Survey of Western Australia, Record 2011/4, 116p.

Huismans, RS and Beaumont, C 2002, Asymmetric lithospheric extension: the role of frictional plastic strain softening inferred from numerical experiments: Geology, v. 30: p. 211–214.

Ord, A, Hobbs, BE and Lester, DR in press, Coupled mineral reactions and fluid flow in hydrothermal systems: Ore Geology Reviews.

Smithies, RH, Howard, HM and Kirkland, CL 2012, The importance of lithogeochemistry to the west Musgrave Province mapping project, *in* GSWA 2012 extended abstracts: promoting the prospectivity of Western Australia: Geological Survey of Western Australia, Record 2012/2, p. 27–29.

Spaggiari, CV, Kirkland, CL, Pawley, MJ, Smithies, RH, Wingate, MTD, Doyle, MG, Blenkinsop, TG, Clarke, C, Ooorschot, CW, Fox, LJ and Savage, J 2011, The geology of the East Albany–Fraser Orogen — a field guide: Geological Survey of Western Australia, Record 2011/23, 98p.

West, JD, Fouch, MJ, Jeffrey, B, Roth, JB and Elkins-Tanton, LT 2009, Vertical mantle flow associated with a lithospheric drip beneath the Great Basin: Nature Geoscience, v. 2, p. 439–444, doi:10.1038/ngeo526.

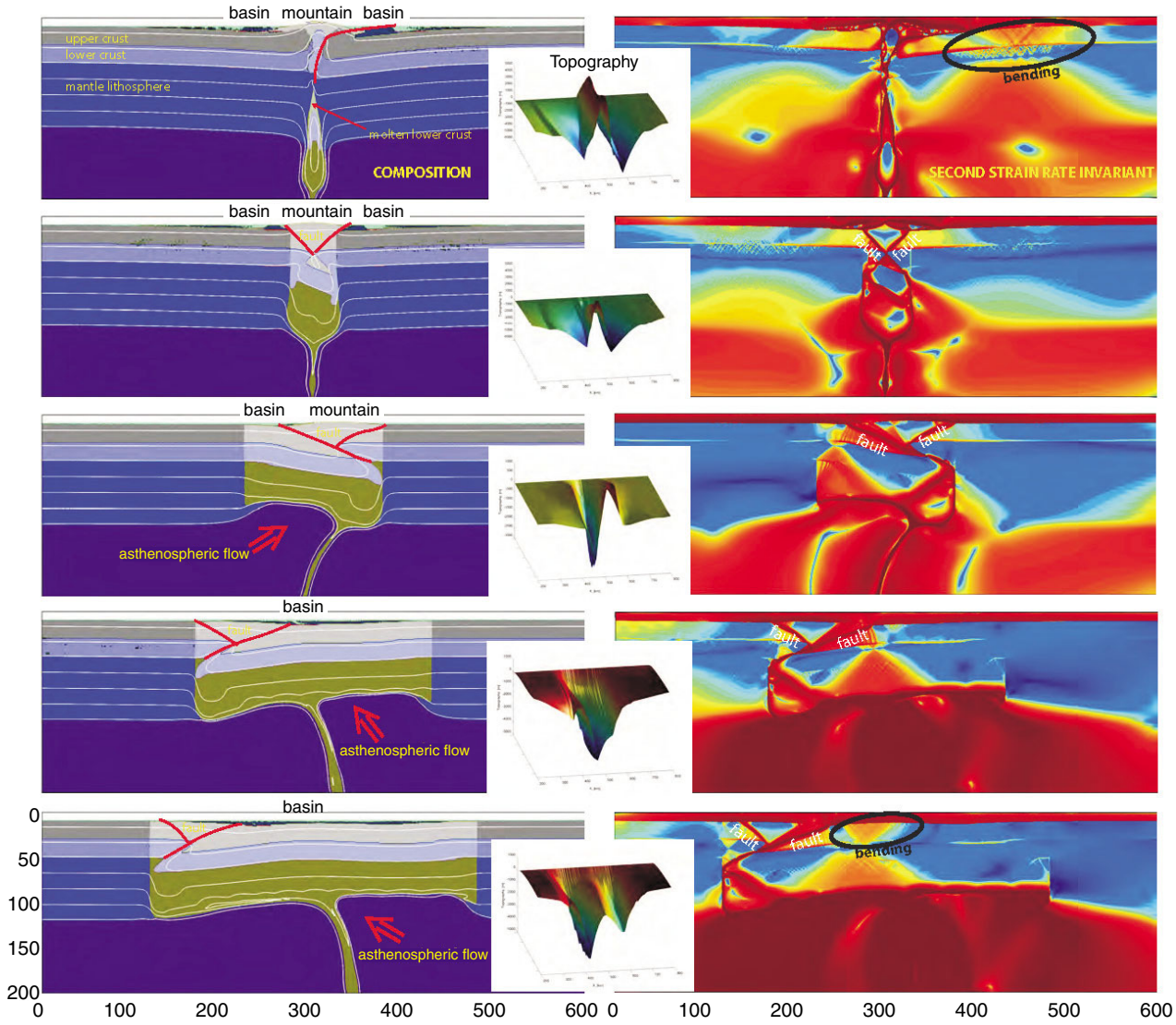

Figure 4. ***Influence of width of SCLM weak zone on the delamination process. Models are 300 km thick in all cases; width of weak zone varies from 50 km at the top to 400 km at the bottom; base of SCLM defined by 1300°C isotherm. Left-hand panel shows the geometry, with the development of Y-shaped fault systems shown in red; right-hand panel shows the distribution of strain rate. Inset shows the development of surface topographic relief.***

RECORD 2012/2

GSWA 2012 EXTENDED ABSTRACTS

Promoting the prospectivity of Western Australia

This Record is published in digital format (PDF) and is available as a free download from the DMP website at <http://www.dmp.wa.gov.au/GSWApublications>.

Further details of geological products produced by the Geological Survey of Western Australia can be obtained by contacting:

Information Centre
Department of Mines and Petroleum
100 Plain Street
EAST PERTH WESTERN AUSTRALIA 6004
Phone: (08) 9222 3459 Fax: (08) 9222 3444
http://www.dmp.wa.gov.au/GSWApublications

GSWA